Ultra-Broadband Fiber-Based Optical Supercontinuum Source

Luo Ma

A Thesis

In the Department

of

Electrical and Computer Engineering

Presented in Partial Fulfillment of the Requirements
for the Degree of Master of Applied Science (Electrical and Computer Engineering) at
Concordia University
Montréal, Québec, Canada

March 2011

CONCORDIA UNIVERSITY
SCHOOL OF GRADUATE STUDIES

This is to certify that the thesis prepared

By: Luo Ma

Entitled: "Ultra-Broadband Fiber-Based Optical Supercontinuum Source"

and submitted in partial fulfillment of the requirements for the degree of

Master of Applied Science

Complies with the regulations of this University and meets the accepted standards with respect to originality and quality.

Signed by the final examining committee:

_____ Chair
Dr. D. Qiu

_____ Examiner, External
Dr. Y.M. Zhang (MIE) To the Program

_____ Examiner
Dr. M. Z. Kabir

_____ Supervisor
Dr. X. Zhang

Approved by: _____
Dr. W. E. Lynch, Chair
Department of Electrical and Computer Engineering

_____20_____ _____
Dr. Robin A. L. Drew
Dean, Faculty of Engineering and
Computer Science

ABSTRACT

Ultra-Broadband Fiber-Based Optical Supercontinuum Source

Luo Ma

The supercontinuum (SC) generation has been studied intensively because of its numerous applications, such as in optical coherence tomography, dense wavelength division multiplexing, ultrafast spectroscopy, and frequency metrology. The SC generation is usually obtained using a highly nonlinear fiber pumped by high power lasers. Two typical pump sources are usually used in SC generation: continuous wave (CW) lasers and ultra-short pulse lasers. The multimode CW lasers are considered as the low-cost pump source, while ultra-short pulse lasers with high peak power can induce nonlinear effects easily in SC generation.

The two pump sources are both considered in this thesis. The first designed SC source contains two low-cost 975 nm multimode CW laser diodes, Erbium/Ytterbium co-doped fiber (EYDF) and highly nonlinear fiber (HNLF), while the other contains a figure-8 mode locking fiber laser, an Er-doped fiber amplifier and photonic crystal fiber (PCF). For the CW laser pumped SC source, the optical spectrum spanning from 900 nm to more than 2000 nm is generated successfully. The total optical output power of SC source is about 200 mW. Additionally, the internal physic mechanisms and reliability of this ultra-broadband SC source are investigated. The ultra broadband and low-cost are achieved simultaneously in this designed source.

For the SC generation using a short pulse laser, PCF attracts the most attention due to its high nonlinearity and flexible dispersion profiles. Here, a picosecond (ps) pulse laser and PCF with flat dispersion are used. We demonstrate a simple and compact all-

fiber supercontinuum source with smooth and fine-structure-free spectrum from 1200 nm to 1920 nm. Furthermore, the pump peak is not observed obviously in the SC spectrum and SC spectrum flatness is better than 11 dB. Related physical mechanisms are discussed. The stability and relative intensity noise (RIN) are also analyzed. The designed SC source has a high smoothness. In particular, the RIN of the broadband SC is comparable to that of the pump laser source.

The two proposed fiber-based optical SC laser sources are simple, compact and practical.

Acknowledgements

First, I would like to express my deepest appreciations to my supervisor, Dr. X. Zhang and co-supervisor, Dr. Zhenguo Lu, senior officer of Institute of Microstructural Sciences (IMS), National Research Council (NRC). Not only they offer precious opportunity to study in NRC, but also give many guidance, professional advices and financial support for me to finish my master thesis.

Second, I am honored to appreciate to Dr. Jiaren Liu, senior officer of IMS, NRC and Dr. Bouchaib Hraimel, the Lab manager of Advance Photonics Lab, Concordia University, for their valuable suggestions and kindly help in my research.

Third, the Advance Photonics Lab members including Zhejing Jiao, Ran zhu, Mario, Yejun Fu, et al offer great help in my research and thesis writing.

Forth, I have sincere appreciation to P. Long, President of O/E land Inc. and J. Carignan O/E land Inc, for their technical support and help on the practical operations in experiment.

Also, thanks to the Canadian Institute for Photonic Innovations and O/E Land Inc., Montreal for supporting this research project.

Last but not least, I really appreciate my parents and my wife Jingfang Liu for their support throughout my life.

Table of Contents

List of Figures

List of Tables

List of Acronyms

ASE	Amplified Spontaneous Emission
CW	Continuous Wave
CDMA	Optical Code Division Multiple Access
CWDM	Coarse Wavelength Division Multiplexing
DWDM	Dense Wavelength Division Multiplexing
DCF	Double-Cladding Fiber (in the combiner)
DSF	Dispersion-Shifted Fiber
EDF	Erbium Doped Fiber
EYDF	Erbium/Ytterbium Co-doped Fiber
FWM	Four-Wave Mixing
GVD	Group Velocity Dispersion
HNL-DFF	Highly-Nonlinear Dispersion-Flattened Fiber
HNLF	Highly Nonlinear Fiber
MI	Modulation Instability
NA	Numerical Aperture
OCT	Optical Coherence Tomography
OSA	Optical Spectrum Analyzer
PCF	Photonic Crystal Fiber
PCE	Power conversion efficiency
RFL	Raman Fiber Laser
RIN	Relative intensity noise
SBS	Stimulated Brillouin Scattering
SC	Supercontinuum

SLED	Superluminescent Diode
SMF	Single Mode Fiber
SPM	Self-Phase Modulation
SRS	Stimulated Raman Scattering
WDM	Wavelength Division Multiplexing
XPM	Cross-Phase Modulation

List of Principal Symbols

A	Ampere
A_{eff}	Effective area (μm^2)
D	Dispersion parameter ($ps/(nm \cdot km)$)
D_M	Material dispersion ($ps/(nm \cdot km)$)
D_W	Waveguide dispersion ($ps/(nm \cdot km)$)
Er	Erbium
g_R	Raman-gain coefficient (m/W)
g_R / A_{eff}	Normalized Raman-gain coefficient $(W \cdot km)^{-1}$
g_B	Brillouin-gain coefficient (m/W)
$\hbar$	Reduced Planck constant ($6.582 \times 10^{-16} eV \cdot s$)
$\hbar\omega$	Photon energy
K_1	Cross relaxation coefficient, energy transfer from Er^{3+} to Yb^{3+}
K_{-1}	Cross relaxation coefficient, energy transfer from Yb^{3+} to Er^{3+}
K_2	Cross relaxation coefficient, secondary energy transfer from Yb^{3+} to Er^{3+}
Δk_M	Phase-matching contribution from material dispersion (cm^{-1})
Δk_{NL}	Phase-matching contribution from waveguide dispersion (cm^{-1})
Δk_W	Phase-matching contribution from nonlinear effects (cm^{-1})
L_{eff}	Effective interaction length (km)
s	Dispersion slope ($ps/(nm^2 \cdot km)$)
$\overline{n_2}$	Nonlinear-index coefficient (m^2/W)

Yb	Ytterbium
λ	Wavelength (nm)
ω	Angular frequency (TH_z)
β	Propagation constant (radians/meter)
α	Fiber loss (dB/km)
β_2	GVD coefficient (ps^2/km)
$\lambda_{ZD}(\lambda_0)$	Zero dispersion wavelength (nm)
γ	Nonlinear coefficient $(W \cdot km)^{-1}$
Ω	Frequency spacing between two lights

CHAPTER 1 INTRODUCTION

1.1 Background and Applications of Broadband Optical Sources

The broadband optical source is attractive because of its widespread applications in optical coherence tomography (OCT), fiber-optic sensing and spectroscopy, coarse wavelength division multiplexing (CWDM) network testing, and frequency metrology [1-4]. Generally, supercontinuum (SC), amplified spontaneous emission (ASE) light, superliminescent diodes (SLEDs) and normal lamp including sunlight and incandescent lamps are considered as broadband optical sources. Figure 1.1 shows the optical spectrum for the corresponding broadband optical source [2]. The typical ASE source resulted from doped fiber, such as Erbium doped fiber (EDF) amplifiers, only covers the C-band and L-band. For the SLED, the optical bandwidth of tens of nanometers and complex configuration limit its applications. Although the sunlight and incandescent have wide bandwidths: 2200 nm and 350 nm, respectively, their optical power levels are too low to be used in practical applications.

Compared with other broadband sources, SC laser is an ideal optical source with ultra-broadband optical spectrum and sufficient power level. The bandwidth of SC is hundreds of nanometers and SC source has been used in optical communications, such as dense/coarse wavelength division multiplexing (D/CWDM), optical code division multiple access (CDMA) and so on. Also, the SC laser source with high spatial coherence and low temporal coherence properties can be used in imaging systems such as optical metrology and OCT [5]. The axial resolution of the imaging system can be improved to

several micrometers by using SC source, which is more precise than using SLED sources. In addition, the SC source has flexible optical spectral coverage from visible to mid-infrared, which is practical for special commercial applications.

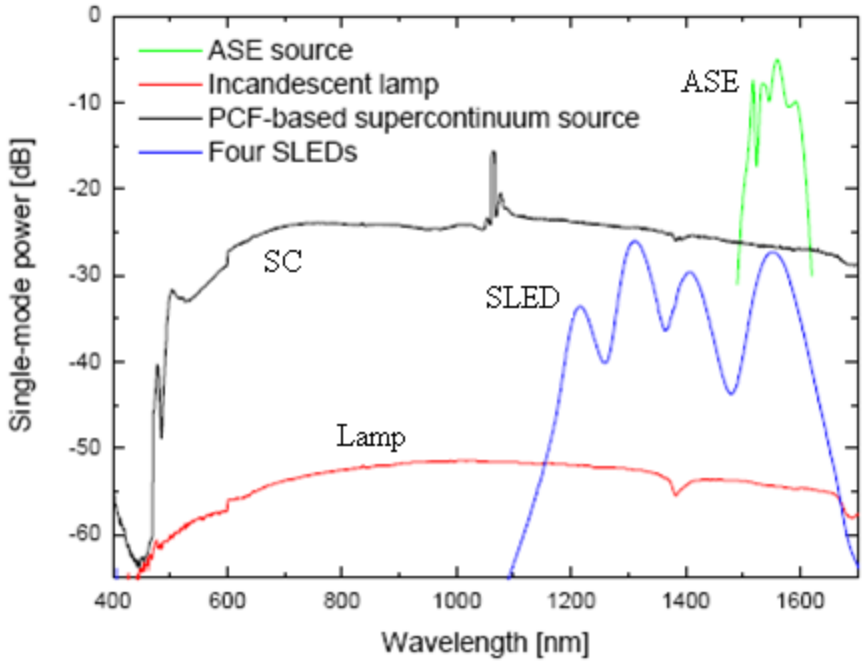

Figure 1.1: Optical spectrum characteristics of four different broadband optical sources [2].

1.2 Review of SC Generation Technologies and Motivation

The spectral broadening is generated from optical nonlinear effects occurring in light propagation [6]. Supercontinuum generation is a typical nonlinear process in which pump laser light propagates in nonlinear fiber and then new frequency components are generated [7]. Typically, the pump sources include pulse lasers from nanosecond to femtosecond and high power continuous wave (CW) lasers. The peak power of a pulse laser is usually very high, which is essential to yield spectral broadening. Also, watt-level CW pump lasers can be used in supercontinuum generation. SC generation has been

investigated intensively since it was first observed in glass [8]. After that, different kinds of waveguides including solids, organic, inorganic liquids, gases and bulk glass were studied to obtain SC spectrum. Compared with other nonlinear media, highly nonlinear fiber (HNLF) and photonic crystal fiber (PCF) with high nonlinearity and appropriate dispersion properties are two practical choices. Their detailed characteristics will be discussed in Chapter 2. Here, we focus on the SC generation using two typical pump sources: ultra-short pulse laser and CW laser.

1.2.1 SC generation using a pulse pump laser

When the short pulse trains with high peak power are injected into PCF or HNLF, various nonlinear effects such as self phase modulation (SPM), four wave mixing (FWM) dispersive wave generation, soliton fission and stimulate Raman scattering (SRS) can be induced to broaden optical spectrum [7]. The internal physic mechanisms are complex because various parameters including the zero dispersion wavelength (ZDW) of PCF, the pump wavelength, pump power level, and particularly the peak power of pulse laser can influence the spectrum broadening processes. Therefore, numerous theoretical and experimental studies have been carried out to analyze the interesting phenomenon. In this section, we will first review the femtosecond (fs) pulse laser pumped SC, and then the longer duration pulse, i.e. picosecond and nanosecond laser pumped SC source.

A: Review of previous SC obtained using femtosecond pulse pump laser

In 2000, a broadband SC from 400 to 1500 nm was first obtained by using Ti:sapphire self mode-locking laser with pulse duration 100 fs pumped PCF at anomalous dispersion wavelength region [9]. The SPM and SRS nonlinear effects were used to explain the flat spectrum broadening. After that, other experimental results have been reported. In particular, the role of soliton fission in SC generation was first demonstrated by Husakou and Herrmann in 2002 [10]. They compared the experimental observations with the theoretical simulations based on nonlinear Schrodinger equation (NLSE) model. Since the theoretical model does not include the role of stimulated Raman scattering, the mismatch occurs in the long wavelength components of SC spectrum. Later, soliton fission and Raman effects were included in generalized nonlinear Schrodinger equation (GNLSE), and matched results between experimental and theoretical analyses were obtained [11, 12]. After that, more detailed results were given by Genty group [13]. The SC generations with pump wavelengths at normal and anomalous dispersion regions were intensively studied [14-16]. It was demonstrated that the pump wavelength close to ZDW is useful to generate broadband SC. In addition, cross phase modulation (XPM) effect plays an important role in the short wavelength components of SC generation, which has been demonstrated experimentally and theoretically [17, 18]. A detailed review of fs pulse laser pumped SC was given in [7]. The theoretical and experimental results were analyzed. It was found that fs laser pumped SC mainly results from SPM effects when pump wavelength is in normal group velocity dispersion (GVD) region; while SC is primarily generated due to soliton fission dynamics when pump wavelength is in anomalous GVD region.

B: SC generation using a picosecond or nanosecond pulse laser pump

In the previous section, the fs pulse laser pumped SC generations were reviewed. In this section, the picosecond (ps) or nanosecond (ns) pulse laser pumped SCs will be discussed in details. Compared with fs pulse, picosecond and nanosecond pulse trains are easily obtained. Additionally, the SC generation mechanisms are different with fs pulse laser pumped broadband sources. The SC spectrum spanning from 400 to 1000 nm was generated by using 60 ps pulse laser and 10m-long PCF with ZDW at 675 nm by Coen et al [19]. Also, SC spectrum from 450 to 750 nm was obtained by using 0.8 ns pulse from Q-switched micro chip laser at 532 nm [20]. The pump wavelengths were in the normal GVD region in the above experiments. Such SC generation primarily results from Raman scattering and four wave mixing (FWM), which have been demonstrated in experiment and numerical studies [21]. For pump wavelength in anomalous GVD region, similar SC results were reported by using nanosecond pump source in 2002 [22]. The generated SC was mostly in infrared region due to cascaded Raman effects. Additionally, broadband SC sources with high power output were reported by using ps pulse laser pump at around 1060 nm [23]. The spectral power densities can be up to mW/nm, which is much higher than the fs pulse laser pumped SC source. These SC results were explained by modulation instability, soliton, associated dispersive waves and Raman scattering nonlinear effects, separately. In addition, a flat SC from 1.35 to 1.7 μm was reported by using a nanosecond pulse laser pump and PCF with two ZDWs [24]. The modulation instability and stimulated Raman scattering are responsible for such SC because of the two ZDWs.

Now, the physic mechanism in pulse laser pumped SC with PCF can be clearly explained by the fact that the short wavelength region of the SC primary results from dispersive wave generation, and the long wavelength region mainly results from soliton fission and Raman self-frequency shift. Many studies also focus on high-quality SC generation besides understanding of physics mechanism. The bandwidth, spectrum flatness, phase stability, and relative intensity noise (RIN) of SC are key parameters in its practical application. A flat-top SC has been demonstrated theoretically by using sub-10fs pulse and all normal dispersion PCF [25]. The detailed study on RIN of SC was given by Corwin group in 2003 [26]. They demonstrated that the chirp of pump pulse is a vital parameter on the RIN of SC. The RIN of SC can be reduced to minimum when the pump pulses are transform limited. In addition, the pump wavelengths of the SC generations mentioned above were mainly in short wavelength region, which were located in 500~1000 nm wavelength window. Recently, SC generation with pump wavelength in optical communication widow around 1550 nm also has been studied. Also, flat SC based on 170 fs mode-locked fiber laser was reported [27]. Although the bandwidth is less than 200 nm, the flat spectrum and high average power output are practical in SC applications. Additionally, special PCFs, such as soft glass PCF and SF6 glass PCF have been used in SC generation in theoretical and experimental studies [28-30]. Particularly, an ultra-broadband SC from 1000 to 2500 nm was obtained by using 100 fs pulse laser and large mode area erbium-ytterbium-doped PCF [31]. These PCF-generated SC source experiences coupling issue of the special PCF to other optical components. In addition, an ultra-boradband source with flat spectrum from 500 to 2400 nm was developed by NKT Photonics Company, which processes a large portion of the broadband source

market [2]. However, the pump wavelength is at 1060 nm, which results in relative expensive system cost. Therefore, it is necessary to generate high quality SC source by using 1550 nm pulse pump laser.

1.2.2 SC generation using continuous-wave pump lasers

Besides pulse laser pumped SC, continuous wave (CW) laser as pump source also can be used to generate SC. The SC with high average output power and 200nm-bandwidth is obtained by using 8.7 W CW pump source and 100m-long PCF [32]. The obtained SC spectrum was explained by cascaded Raman scattering. After that, the roles of modulation instability and four-wave mixing were also demonstrated in SC generation based on cascaded Raman fiber laser and HNLF [33]. Also, some CW laser pumped SCs mainly from FWM processes were reported [34]. Since the peak power of CW laser source is low, the high average power CW laser is required to induce nonlinear broadening. Because of high-power operation requirement, use of Raman fiber laser is not considered a low-cost solution. Fortunately, multimode CW laser diodes provide a new possibility to generate low-cost SC source. The low- cost SC from 1300 to 1750 nm was first obtained by using two 975 nm multimode pump lasers and HNLF in a ring structure in 2006 [35]. The SC evolution with respect to pump power was given. In addition, they analyzed the long term stability and RIN features of SC. However, the SC output power is only tens mili-watts. In 2007, our group obtained a SC from 1550 to 1900 nm by using a similar configuration [36]. Also, a Watts-level broadband SC source was obtained by optimizing splitting ratio of the ring configuration [37]. In addition, the ultra-broadband SC from 1200 to 2000 nm was also observed in a single-line structure [37].

The normal fiber usually has high loss after 2000 nm, which can limit SC further extension. Hence, the multimode CW laser pumped SC source in short wavelength region needs more investigations.

1.3 Thesis Scope and Contributions

The focus of this thesis is to design low-cost and practical ultra-broadband laser sources. Two kinds of pump lasers: multimode CW laser and short pulse laser are considered. In the CW laser pumped SC, two 975 nm multimode CW lasers, 8m-long Erbium/Ytterbium co-doped fiber (EYDF) and 1.21km-long HNLF are used. The designed system can generate ultra-broadband continuum spanning from 900 to 2000 nm. The evolution process, output optical power, and long term stability are investigated. Corresponding nonlinear effects in the broadening process are also analyzed. In the second scheme, picosecond pulse trains are first generated from home-made Erbium-doped Raman fiber laser, and amplified further by Erbium doped Fiber Amplifier (EDFA), then injected into PCF. A flat and broadband SC source from 1200 to 1900 nm is obtained successfully. This broadband source is compact and simple. This work on SC generations presents practical guide in future research and can develop more application in optical communication.

The main contributions of this work are given as follows:

1. Design and fabricate a low cost and ultra-broadband CW-pumped SC fiber laser experimentally. It is the first report on SC source extending from 900 to 2000 nm using 975-nm multimode pump laser diodes. The long-term stability of this source is discussed.

2. Propose and design a flat and broadband pulse laser pumped SC source, which covers from 1200 to 1900 nm. The SC source with 11dB-flatness presents stable and fine structure free. Particularly, the pump peak disappears in the final SC output. In addition, the long-term stability and RIN feature are also analyzed. The RIN of broadband SC source is comparable to the pulse pump laser.

1.4 Thesis Outline

The organization of this thesis is presented in this section.

Chapter 2 presents the experimental model of SC source using CW pump lasers and a short pulse pump laser, respectively. The functions of doped fiber and nonlinear fiber are introduced. The nonlinear effects and generation mechanisms are given in details.

Chapter 3 shows the CW laser pumped SC generation in a single-line structure. The backward amplified spontaneous emission (ASE) as seed light is used to induce SC broadening. The ultra-broadband optical source from 900 to 2000 nm is generated. The evolution processes and the long-term stability are discussed in details.

Chapter 4 illustrates SC sources by using a picosecond pulse laser and PCF with flat dispersion. The nonlinear broadening processes are analyzed in details. The SC output in time domain is also given. In addition, the long term stability and RIN characteristics are investigated.

Chapter 5 gives the conclusions of this thesis and future work.

CHAPTER 2 CONFIGURATIONS OF SC GENERATION AND THEORETICAL ANALYSIS

In this chapter, two different models of SC source are first presented. Then the principle of SC generation and nonlinear effects are introduced. In addition, the related roles of Er-Yb doped fiber, HNLF, and PCF are analyzed in details.

2.1 Introduction of Experimental Setup

The CW laser pumped SC source in a single-line structure is depicted in Figure 2.1. The broadband source mainly includes CW pump laser, doped fiber, and highly nonlinear fiber. Compared with the ring structure, the single-line SC configuration with the minimum bandwidth limitation has the potential to obtain maximum broadband spectrum. In addition, such SC generation source is simple, easy to assemble, and compact. The general principle of the SC generation is introduced as follows. Firstly, the high power 975 nm light generated from multimode CW pump laser is launched into the doped fiber and then is converted to ASE light around 1550 nm as seed beam. After that the seed beam propagates in nonlinear fiber. Then various nonlinear effects are induced and the spectrum is broadened significantly. Finally, the SC output can be obtained. The related functions of the doped fiber and nonlinear fiber will be discussed in the following sections. The other broadband SC source is pumped by short pulse laser, as shown in Figure 2.2. The short pulse trains with high peak power around 1550nm are injected into PCF directly. As numerous nonlinear effects occur, broadband SC spectrum can be achieved eventually. In addition, the characteristics of PCF will be discussed in details.

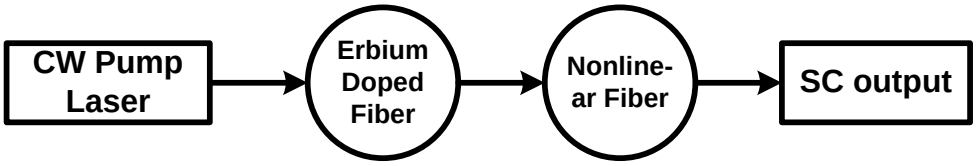

Figure 2.1: Experimental setup of CW laser pumped SC laser.

Figure 2.2: Experimental setup of a short pulse laser pumped SC source.

2.2 Erbium doped Fiber and Erbium (Er)/Ytterbium (Yb) Co-doped Fiber (EYDF)

In this section, the detailed characteristics of the doped fiber will be introduced. The doped fiber is an essential component in the CW laser pumped SC source and it can convert 975 nm pump light into 1550 nm seed light. Here, Erbium/Ytterbium Co-doped fiber is used to obtain high power ASE in our SC generation source, which will be given in details.

2.2.1 Characteristics of Erbium doped fiber

Erbium is a type of rare earth material, and it is often used as gain medium in lasers or optical amplifiers. Among the internal transitions of Er^{3+}, the main transition used is between manifold $4I_{13/2}$ and ground state manifold $4I_{15/2}$, as shown in Figure 2.3 [38]. Er^{3+} can absorb 980 nm pump light and transfer it to long wavelength light in Erbium doped fiber. This transition can emit the light with wavelength nearby 1550 nm, and it corresponds to the typical optical communication window. Particularly, this wavelength

is close to the ZDW of nonlinear fiber. However, the absorption efficiency for 975 nm pump light is relatively low in Er doped fiber because of the small cross section and limited doping concentration. The absorption efficiency can be improved by co-doping with other rare earth metals, such as the most common used element: Ytterbium and this will be discussed in next section.

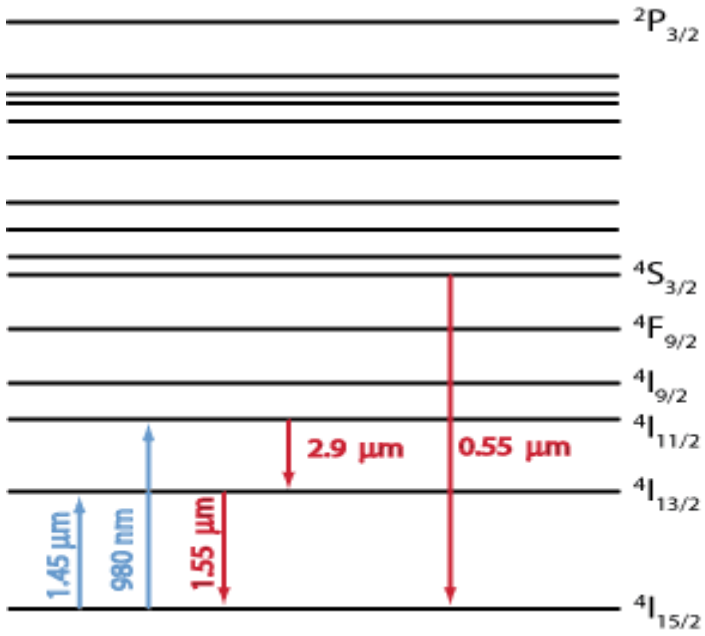

Figure 2.3: Energy level diagram of Erbium element [38].

2.2.2 Characteristics Er-Yb co-doping fiber (EYDF)

Firstly, the definition of Er-Yb co-doping fiber is given. Both Erbium and Ytterbium elements are doped in the core of optical fiber simultaneously, and such fiber is usually named as Er-Yb co-doped Fiber or Er-Yb doped Fiber. Here, we define it as EYDF in short. Since the two rare earth elements have adjacent resonant energy levels, particles exchange can occur in EYDF. The energy level $^4I_{11/2}$ of Er^{3+} and $^2F_{5/2}$ of Yb^{3+} are resonant energy levels, as shown in Figure 2.4 [39]. Yb ion can absorb CW light more efficiency

than Er^{3+} in 975 nm wavelength region. Therefore, Yb^{3+} ions is used to absorb pump light and Er^{3+} ions emit 1550 nm light by stimulated or spontaneous emission process in co-doping fiber.

From the energy level diagram in Figure 2.4, three primary cross-energy conversion progresses in EYDF can be observed. The related cross relaxation coefficients are defined as K_1, K_{-1} and K_2, respectively.

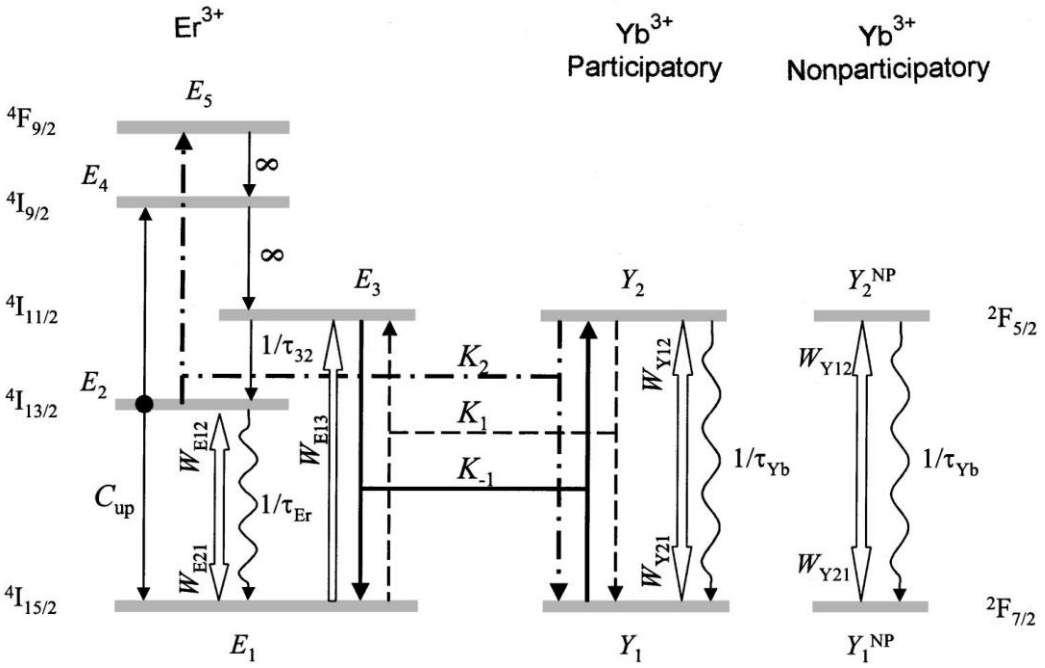

Figure 2.4: Energy transition diagram of Erbium and Ytterbium [39].

The coefficient K_{-1} describes the interaction process as follows. Firstly, particles at the ground state: ${}^2F_{7/2}$ of Yb^{3+} absorb the pump light and then are raised to the excited state: ${}^2F_{5/2}$. Then, the particles will transfer to the closed resonant energy level of Er^{3+}. Finally, photons can be emitted by spontaneous emission or stimulated emission from ${}^4I_{11/2}$ energy level to ground state ${}^4I_{15/2}$ of Er^{3+}.

The opposite energy transition progress is identified by the coefficient K_1. The Er^{3+} particles are pumped from ${}^4I_{15/2}$ to the excited energy state ${}^4I_{11/2}$. After the conversion between resonant energy levels, particles fall to ground state of $Yb^{3+}:{}^2F_{7/2}$ by emitting photons. Note that the absorption of Er ions on 975 nm light is suppressed significantly due to the existing Yb ions in EYDF.

The third energy transition process is named as the coefficient K_2. It includes two different transition processes. First, the particles of Ytterbium ions at ${}^2F_{5/2}$ level fall to ${}^2F_{7/2}$ without resonant energy conversion. The second progress happens in Erbium ions: particles in energy state ${}^4I_{11/2}$ nonradioactive decay to ${}^4I_{13/2}$ and then are pumped to higher energy level ${}^4F_{9/2}$. Such energy state transitions will reduce the conversion and amplification efficiencies of the 1550 nm seed beam. In addition, other interactions between the particles and the pump light also exist simultaneously. Compared with the main three processes, these interactions can be ignored.

2.2.3 Functions of Er-Yb co-doping in EYDF

Three main advantages of Er-Yb co-doping fiber are reviewed in this section.

1) **Broad absorption band**

Compared to Erbium doped fiber, Ytterbium ions in Er-Yb co- doping fiber can broaden the absorption band from 800 to 1100 nm. Therefore, available pump sources within this wavelength window can be used such as 975 nm multimode CW laser and 1064 nm Nd:YAG laser.

2) Higher Er doping concentration

Generally, the Erbium doped fiber has a threshold value for the doping concentration. The limited doping concentration can limit the effective absorption of the pump light and the gain of 1550 nm seed light. This can be explained by the fact that high doping concentration of Er ions will form clusters and it turns out into concentration quenching. When two adjacent Er ions are very close, the particles at $^4I_{13/2}$ will interact with each other. The process is named as cooperative up-conversion. It describes the fact that one particle falls to the ground state while the other one is firstly excited to $^4I_{9/2}$ level, and then non-radioactively decays to $^4I_{13/2}$ state. The cooperative up-conversation will decrease the conversion efficiency significantly in EDF. However, this problem can be solved by co-doping Yb ions in Er doped fiber. The Yb ions can separate Er ions from each other, which can increase the doping concentration of Er ions. Therefore, the conversion efficiency can be improved in Er-Yb co-doping fiber.

The gain and absorption characteristics of Er ions in EYDF curves are depicted as a function of wavelengths in Figure 2.5. Even the particles cannot be transferred completely from Yb^{3+} to Er^{3+} in EYDF, the absorption peak of Er ions at 1530 nm can reach up to 30 dB/m, which is much higher than normal EDF in C-band or L-band optical amplifiers.

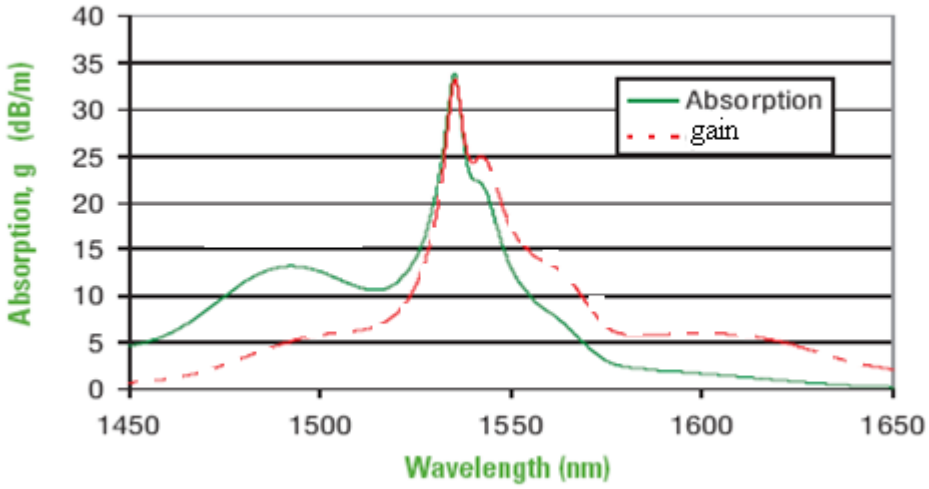

Figure 2.5: Gain and absorption characteristics of Er ions in the EYDF [40].

3) Higher pump power absorption in EYDF

Generally, the pump light propagates in the core area of rare-earth doped fiber. Because of the small core size (only 8μm), the pump power is limited to hundreds milliwatts. However, cladding-pumping is highly efficient and can reach watts-level pump. Here, multimode pump lasers and double cladding fiber (EYDF) are used in our proposed scheme. In this design, pump light could propagate in first-cladding and fiber core simultaneously. The light in the cladding will couple into the fiber core gradually and then it propagates along the fiber core. Figure 2.6 presents the propagation diagram of Er/Yb co-doped fiber [41]. It can be observed that the absorption efficiency is improved significantly due to larger propagation area and the star shape of the EYDF. However, since the unique shape of the fiber increases the difficulty of splicing process, special splicing program is required.

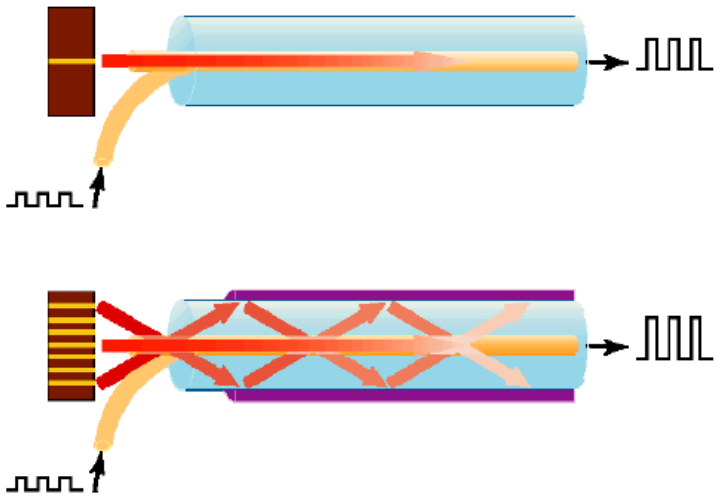

Figure 2.6: Comparison of cladding-pump fiber and conventional core-pump fiber [41].

2.3 Nonlinear Optical Fiber: Highly Nonlinear Fiber (HNLF) and Photonic Crystal Fiber (PCF)

Nonlinear optical fiber is the most important component in the SC generation system. The new frequency components are generated in nonlinear fiber based on various nonlinear effects. And then, spectral broadening is obtained. In this section, the HNLF and PCF are mainly reviewed in details.

2.3.1 Properties of Highly Nonlinear Fiber (HNLF)

Compared with the traditional single mode fiber (SMF), the size of fiber core is smaller and the refractive index difference: Δ between the core and cladding is larger in HNLF. These characteristics can be realized by heavy doping with germanium element. The HNLF has high nonlinearity due to these special designs, as shown in Table 2.1.

Table 2.1: Comparison of HNLF and SMF Nonlinear Parameters [42].

Parameters	HNLF	SMF
Kerr coefficient(n_2)	$4-6(\times 10^{-20} m^2/W)$	$3(\times 10^{-20} m^2/W)$
Effective area(A_{eff})	9-20 (μm^2)	80 (μm^2)
Nonlinear coefficient(γ)	10-30	1.5
Attenuation at 1550nm(α)	0.5-1 (dB/km)	0.2 (dB/km)
Zero dispersion wavelength(λ)	>1350(nm)	1310(nm)

The high nonlinear coefficient: γ and small effective area: A_{eff} are key parameters in the phase shift of self-phase modulation (SPM), threshold of stimulated Raman scattering (SRS) and side bands positions of modulation instability (MI). The two factors are improved significantly in HNLF, which can be seen in Table 2.1. The small A_{eff} of the HNLF is useful to confine the light while attenuation maintains at a certain level. Also the Kerr coefficient: n_2 of the HNLF is higher than in SMF since the fiber core is heavily doped by Ge ions. The high nonlinear coefficient (γ) can be obtained from Kerr coefficient and small effective in the HNLF area. The formula is given as:

$$\gamma = 2\pi \overline{n_2} / (A_{eff} \lambda) \qquad (2.3.1.1)$$

Correspondingly, the nonlinear characteristics of HNLF are greatly enhanced. In next section, we will review three leading types of HNLF.

- **Three different Types of Highly Nonlinear Fibers**

Generally, three main types of HNLFs designed for related applications are commonly mentioned as shown in Figure. 2.7.

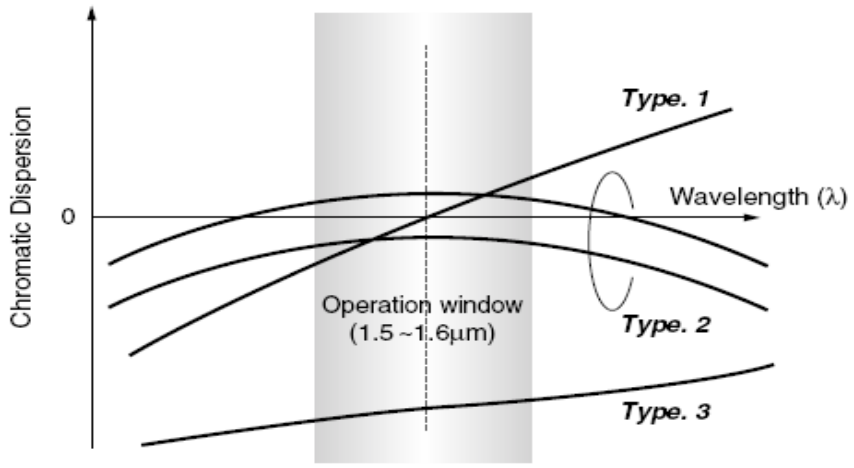

Figure 2.7: Dispersion characteristics of three types of HNLFs [43].

The three different HNLFs are identified by varies dispersion properties. In type-1, the dispersion performance is comparable with the dispersion-shifted SMF. The zero dispersion wavelength: λ_0 is at around 1550 nm, and the dispersion slope is positive. Since the FWM and cross-phase modulation (XPM) are easy to generate in this kind HNLF, it is often applied in wavelength conversion or parametric amplification. The details were given in literature [43], as seen in Figure 2.8. When one pump and one signal are input into the HNLF, an idler light at different frequency is presented. The frequency spacing: Δf between the pump and the newly generated light is the same as that between the pump and the signal, which can be explained by FWM. The frequency spacing is inversely with the intensity of the idler light. In addition, the wavelength of pump light should be in the anomalous dispersion region of the HNLF, and is close to the zero dispersion wavelength.

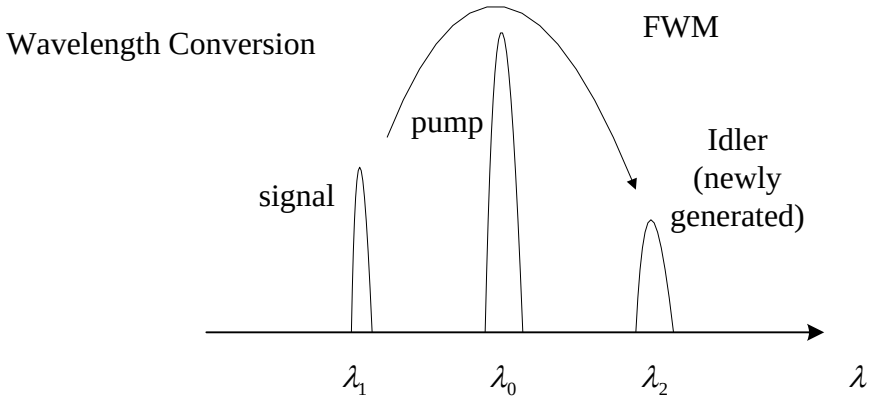

Figure 2.8: Illustration of wavelength conversion by FWM [43].

The dispersion of type-2 HNLF is very flat in the optical communication window 1500-1600 nm. The fiber dispersion maintains a small value in a large wavelength region (1.3-1.6 μm). In addition, the dispersion slope: s alters from positive to negative within this flat region. This kind nonlinear fiber is also named as highly-nonlinear dispersion-flattened fiber (HNL-DFF). It has been demonstrated that many nonlinear effects can be induced to generate supercontinuum in this kind of HNLF, as illustrated in Figure 2.9.

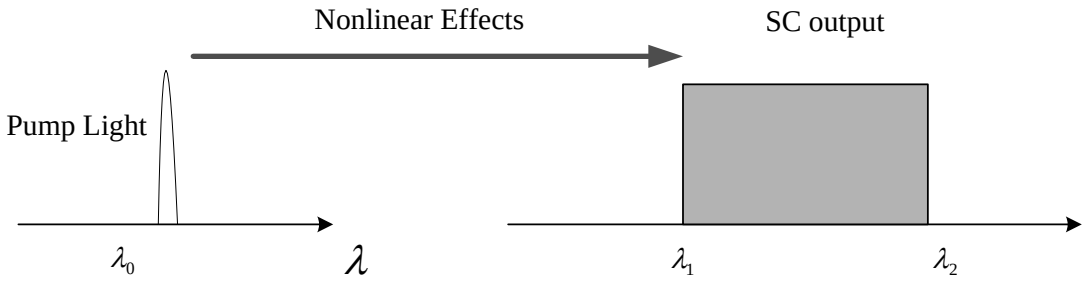

Figure 2.9: Generation of SC by nonlinear effects in Type-2 HNLF [42].

Type-3 HNLF has distinctive dispersion property. As shown in Figure 2.7, it has the big negative dispersion, while dispersion slopes remain small values around 1550 nm. FWM and MI can hardly occur in such HNLF due to phase-mismatching condition.

However, this kind HNLF maintains low attenuation and highly normalized Raman gain coefficient g_R / A_{eff} characteristics, which is useful in Raman amplification. Generally, the parameter g_R / A_{eff} is dependent on the fiber core composition and doping elements, which will be reviewed in details later. The normalized Raman gain coefficient of the HNLF is much higher than other types of fibers, as shown in Figure 2.10.

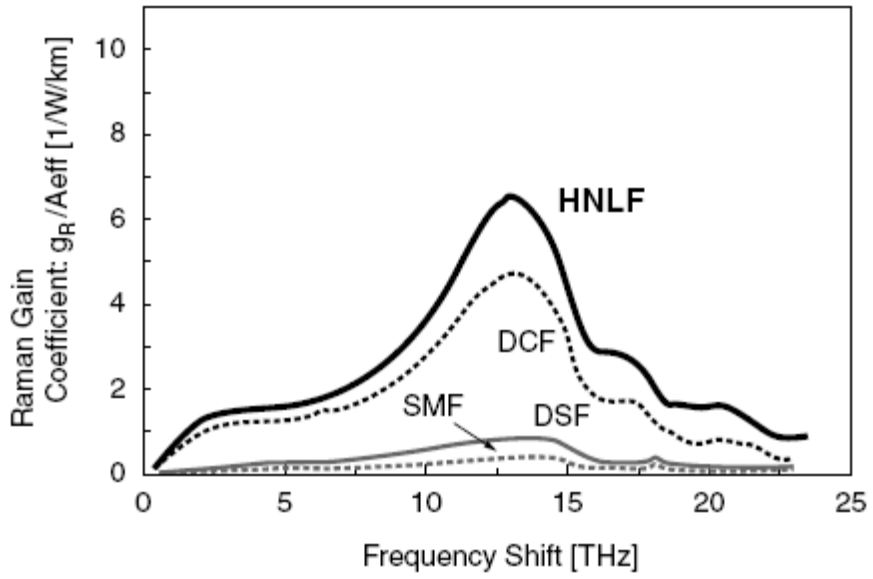

Figure 2.10: Comparison of the coefficient g_R / A_{eff} : of SMF, DCF, DSF and HNLF for Raman effect [43]. SMF, DCF, and DSF represent single-mode fiber, dispersion compensation fiber and dispersion-shifted fiber, respectively.

- **HNLF used in our SC source**

In our experiments, the parameters of the HNLF from Sumitomo Inc. are given in Table 2.2. The ZDW: λ_0 can be estimated by using the formula: $D = S(\lambda - \lambda_0)$. For our HNLF, λ_0 is at 1576.67 nm.

Table 2.2: Parameters of the HNLF used in the experiment [37].

HNLF parameters		Values
Length(m)		1210
Cut-off wavelength λ_c (nm)		1550
Nonlinear coefficient $\gamma(W \cdot km)^{-1}$		12(for random polarization state)
At 1550nm	Dispersion parameter D $ps/(nm \cdot km)$	-0.8
	Dispersion slope S $ps/(nm^2 \cdot km)$	+0.03
	Attenuation α (dB/km)	0.54
	A_{eff} (μm^2)	10
g_R / A_{eff} $(W \cdot km)^{-1}$		6.18
Fiber pigtail (both ends)		SMF
Connector (both ends)		SC/PC
Adaptor (both ends)		SC

2.3.2 Characteristics of Photonic Crystal Fiber (PCF)

PCF comprises a small silica core with high index, which is surrounded by many air-filled cladding holes along the whole length of fiber. The refractive index of the hybrid air-silica material is lower than the core, as seen in Figure 2.11. PCF is also named as other terminologies: microstructure fiber or holey fiber in different literatures [9, 12, 15].

Compared with other fibers, PCF with special design can guide the light with single-mode propagation. Also, the nonlinearity, mode confinement and group velocity dispersion (GVD) all can be engineered by related fiber microstructure. Such type of fiber has significant advantages in SC generation. Additionally, the zero dispersion wavelength can shift from the visible to near-infrared wavelength region, while the ZDW of HNLF is usually over 1350 nm. The pump laser used must be adjusted according to the ZDW of the nonlinear fiber, which has been demonstrated in literature [44], as shown in Figure 2.12. The corresponding zero dispersion wavelengths of the PCF and HNLF are located at around ~800 nm and ~1550 nm, respectively. Therefore, two pump lasers with different operation wavelengths were used. It is mentioned that pump wavelengths in the anomalous dispersion region of PCF could generate broader supercontinuum [37].

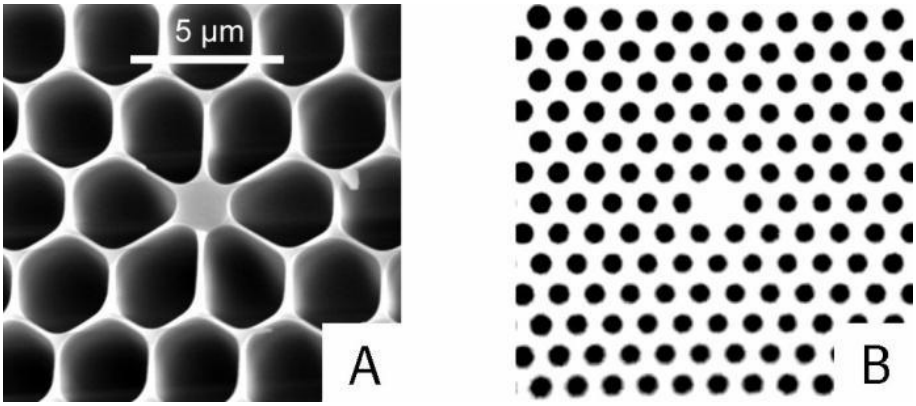

Figure 2.11: Micro-structure of PCF with central solid-core and surrounding air holes [2].

PCF has attracted numerous attentions due to its superior performances in SC generation. Related experiments have been demonstrated that both of the pulse laser and the high power continuous wave (CW) sources can be used to pump PCF and generate SC [7]. PCF-generated supercontinum has been applied widely in optical coherence tomography, spectroscopy, and optical frequency metrology.

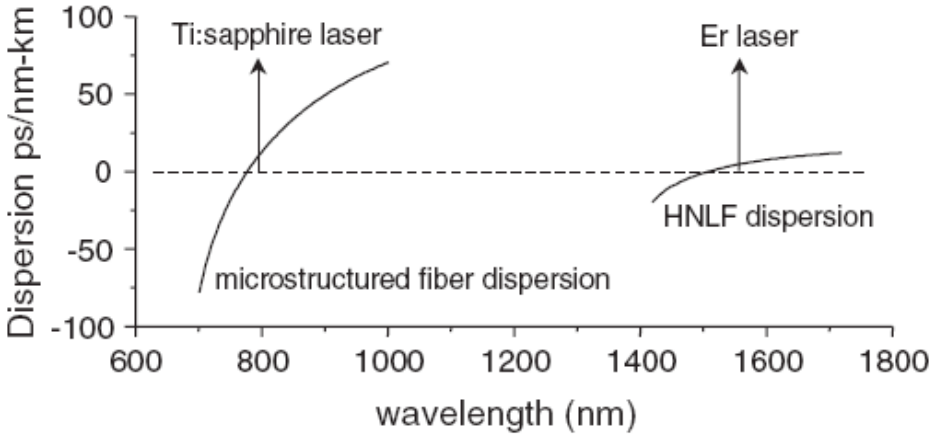

Figure 2.12: Dispersion properties curve of PCF and HNLF [44].

In our experimental setup, the PCF with flat dispersion is NL-1550-POS-1 fiber and from NKT Photonics. The flat dispersion between two ZDWs is essential to generate flat broadband spectrum. The dispersion characteristics are given in Figure 2.13. Many studies have demonstrated that FWM and MI are useful to flatten the spectrum [25, 27-29]. The detailed information of the PCFis given in the Appendix A.

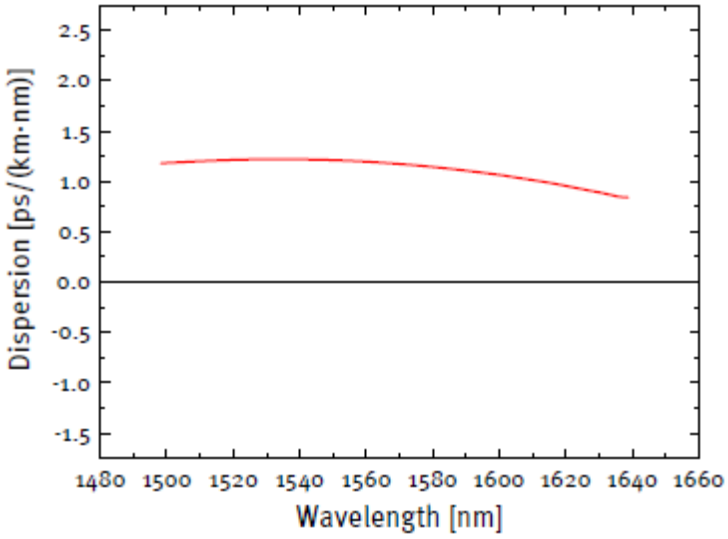

Figure 2.13: Dispersion profile of photonic crystal fiber with two ZDW [45].

2.3.3 Comparison of Highly Nonlinear Fiber and Photonic Crystal Fiber

The comparison of the HNLF and PCF are shown in Table 2.3. It can be seen that the nonlinear coefficient of PCF is up to $100\,(W \cdot km)^{-1}$ due to its special microstructure, which is much higher than HNLF. While the insertion loss and splicing loss of the HNLF are much lower than PCF. Although, the cost of the PCF is much higher than the HNLF, the length of the PCF used in SC generation is only several meters, which is much shorter than kilometers-long of HNLF required in CW pumped SC.

Table 2.3: Comparison of HNLF and PCF.

	HNLF	PCF
Advantage	• High nonlinearity: $10-30(W \cdot km)^{-1}$ • Splicing with low loss to SMF (0.2dB at 1550nm) • Low attenuation	• High nonlinearity: $10-100(W \cdot km)^{-1}$ • Flexible in controlling the dispersion profile • Short length required
Disadvantage	• Chromatic dispersion tailored within limited wavelength range	• High loss • Difficulty to manufacture

2.4 Dispersion and Nonlinear Effects

The group velocity dispersion, SPM, XPM, SRS, SBS, MI and FWM are discussed in this section.

2.4.1Group-velocity dispersion (GVD)

The group velocity dispersion is an optical phenomenon which describes the relationship of the light's group velocity and the optical frequency within propagation. It can be expressed precisely in the following equation:

$$GVD = \frac{\partial}{\partial \omega}\frac{1}{\upsilon_g} = \frac{\partial}{\partial \omega}\left(\frac{\partial k}{\partial \omega}\right) = \frac{\partial^2 k}{\partial \omega^2} \tag{2.4.1.1}$$

In optical fibers, the GVD in terms of wavelength is usually considered. The calculation is given bellow:

$$D_\lambda = -\frac{2\pi c}{\lambda^2}\cdot GVD = -\frac{2\pi c}{\lambda^2}\frac{\partial^2 k}{\partial \omega^2} \tag{2.4.1.2}$$

It can be observed that GVD and D_λ have opposite signs because of the inverse relationship of wavelength and frequency. Avoiding confusion, the terms normal dispersion and anomalous dispersion are preferred to identify them. Furthermore, the dispersion mainly includes material dispersion and waveguide dispersion, as given by

$$D = D_M + D_W \tag{2.4.1.3}$$

Material dispersion depicts the dependency of refraction index of the fiber core on light wavelength, while waveguide dispersion describes the propagation distribution of

different wavelengths: short wavelength light is mainly restricted in the core region; certain part of the light is in the cladding for the long wavelength, which can induce different propagation velocities. Since the two types of dispersions have opposite signs in certain wavelength region, the zero dispersion wavelength: λ_{ZD} can be obtained in optical fiber. For $\lambda < \lambda_{ZD}, D < 0$, the optical fiber shows normal dispersion; when $\lambda > \lambda_{ZD}$ and $D > 0$, the optical fiber turns to the anomalous dispersion mode. Particularly, the anomalous dispersion region is critical for nonlinear optics [42, 43]. The dispersion curves of a stranded single-mode optical fiber as a function of wavelength are shown in Figure 2.14. For this fiber, λ_{ZD} is at 1.31μm. Since high-order dispersion is determined by the dispersion slope: $s = dD/d\lambda$, the dispersion is not exactly zero. In addition, waveguide dispersion can be engineered by altering the fiber index profile, which can be used to compensate material dispersion, to control and shift the total fiber dispersion. In optical communication, λ_{ZD} is often shifted to 1.55 μm because the silica fiber loss has a minimum window near 1.55 μm. Such fibers are often named as dispersion-shifted fibers (DSF).

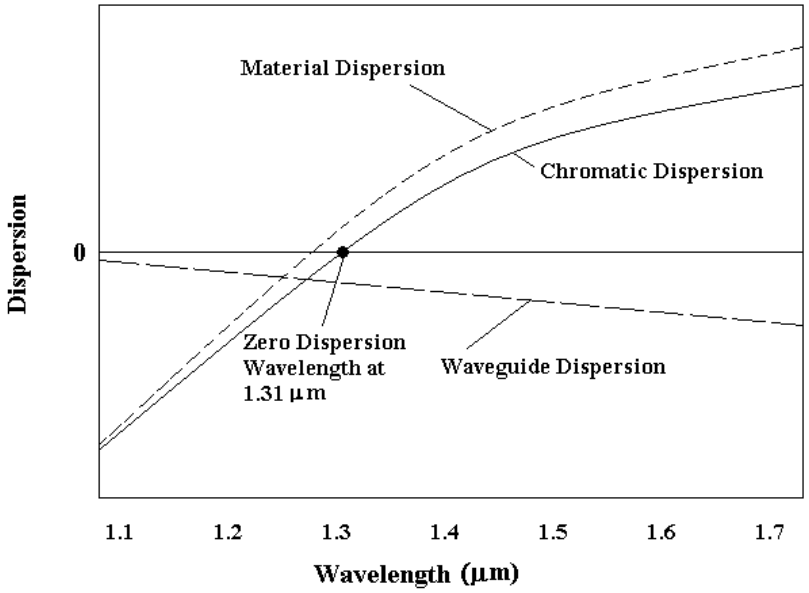

Figure 2.14: Various dispersion characteristics for a conventional single mode fiber [46].

2.4.2 Self-phase modulation (SPM) and cross-phase modulation (XPM)

In optical fiber, high intensity light can induce phase delay due to Kerr effect, which can result in nonlinear change of the refractive index $\Delta n = n_2 I$, where n_2 is fiber refractive index and I is the intensity of incident light. The modification of the fiber refractive index can induce nonlinear dispersion and consequently nonlinear phase shift of optical signal, which is known as self-phase modulation (SPM). The role of the SPM in spectrum broadening can be seen by the following derivations. Refractive indices are described as:

$$n_j^{'} = n_j + \Delta n = n_j + \overline{n_2}(p / A_{eff}), j = 1,2, \qquad (2.4.2.1)$$

where j stands for cladding or core. The parameters: $\overline{n_2}$, P and A_{eff} represent the nonlinear-index coefficient, optical power and effective area of optical fiber, respectvely. Because of the change in refractive index, the propagation constant: β is also modified as:

$$\beta^{'} = \beta + k_0 \overline{n_2} P / A_{eff} = \beta + \gamma P, \tag{2.4.2.2}$$

where $\gamma = 2\pi \overline{n_2} / (A_{eff} \lambda)$ is the nonlinear coefficient, and this can induce nonlinear phase shift ϕ_{NL}.

$$\phi_{NL} = \gamma P_{in} L_{eff}, \tag{2.4.2.3}$$

where L_{eff} is the effective interaction length given as

$$L_{eff} = [1 - \exp(-\alpha L)] / \alpha \tag{2.4.2.4}$$

where α is the fiber loss factor.

Generally, the output power of laser diode: P_{in} is not a constant value and varies with time, which can generate frequency shift:

$$\delta\omega(t) = -d\phi_{NL} / dt. \tag{2.4.2.5}$$

Frequency shift $\delta\omega$ changes with time and this self-induced frequency chirp will broaden the optical spectrum significantly under certain conditions. An example of spectral broadening caused by SPM effect is given in Figure 2.15.

In addition, because of the nonlinear effect of SPM, an unchirped optical pulse can end-up to a so-called chirped pulse. The variation of instantaneous frequency of a pulse along the time course is presented in Figure 2.16. The chirp resulted from SPM can be balanced by the anomalous chromatic dispersion of optical fiber, which is useful to form optical solitons. When the optical signals propagate as fundamental solitons, the spectral width will not be broadened in time domain.

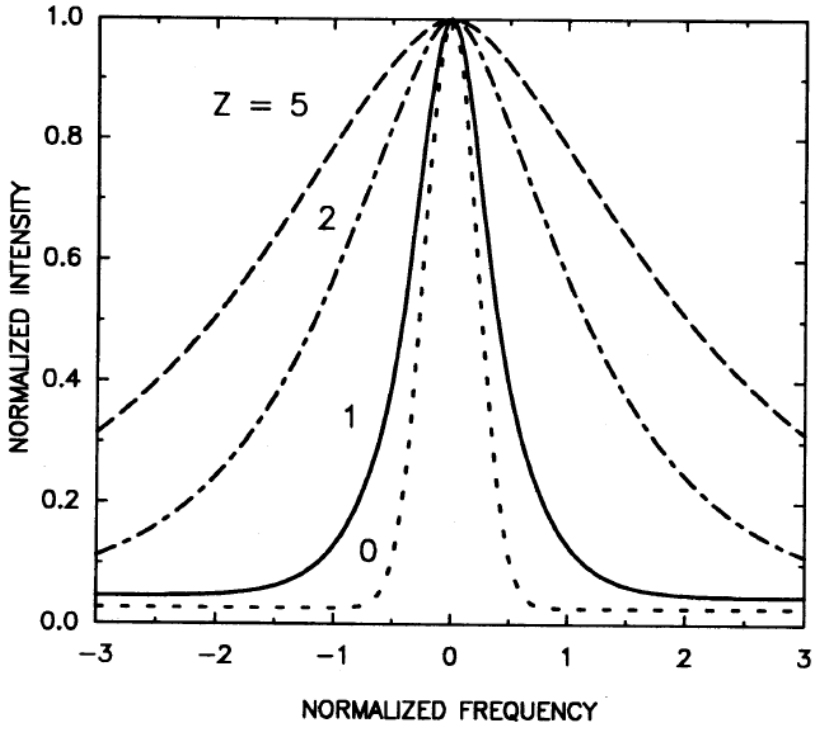

Figure 2.15: Spectral broadening of a CW beam induced by SPM as a function of propagation distance Z [6].

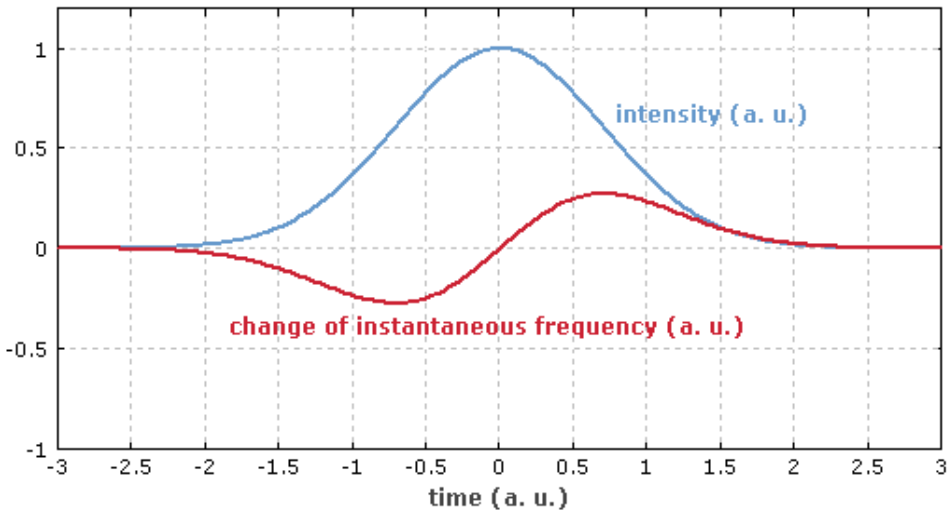

Figure 2.16: Instantaneous frequency of an experienced self-phase modulation and initially unchirped pulse [47].

Cross- phase modulation (XPM) is another nonlinear effect that describes the phase change of a light beam by another light with different frequency. The nonlinear phase shift can be reflected in refractive index:

$$\Delta n^{(2)} = 2n_2 I^{(1)} \tag{2.4.2.6}$$

where n_2 is the refractive index. Here, the function describes that the intensity of beam 1: $I^{(1)}$ results in a change of the refractive index of beam 2. Note that the equation has an additional factor of 2, which is different with the corresponding expression in SPM section. The factor 2 is just applied when the beams have same polarization, while the factor is 2/3 for the beams with cross polarizations.

2.4.3 Stimulated Raman scattering (SRS) and stimulated Brillouin scattering (SBS)

When optical wave interacts with the material, an inelastic scattering of light can be produced. This phenomenon is named as Raman Effect. Generally, when incident photons interact with the material, it can be scattered in three different ways: Rayleigh scattering, Stokes scattering and anti-Stokes scattering. Rayleigh scattering is an elastic scattering and the photons frequency remains the same as the incident light. Stokes scattering and anti-Stokes scattering are inelastic Raman scattering and can cause frequency shift, and because of that, they have attracted many attentions. In most mediums, Raman scattering is weak and hardly observed. However, Raman scattering effect can be generated significantly in optical fibers because high optical intensity densities and long interaction length will enhance the nonlinearity. When the threshold condition is satisfied, both stimulated Raman scattering (SRS) and stimulated Brillouin

scattering (SBS) can be generated. Stimulated scattering condition can convert the pump light to the scattered Stokes wave more effectively. In SRS, the Stokes wave with typical frequency shift in the range of 10^{12}-10^{13} Hz propagates in the fiber along with the pump light. Figure 2.17 shows a typical Raman gain spectrum. The frequency of Stokes wave can be up to ~40THz and the gain peak is around ~13 THz. Also, optical wave with higher frequency than pump light can be produced by Raman anti-Stokes effect. Raman anti-Stokes effect describes the scattering process of photons gaining energy from the medium. The particles in atomic system of medium decay from excited state to ground state and provide energy to the optical beam. Generally, anti-Stokes frequency shift is shorter than Stokes waves and hardly observed in Raman applications. Generally, both Stokes waves and anti-Stokes waves can contribute to spectrum broadening in SC generation.

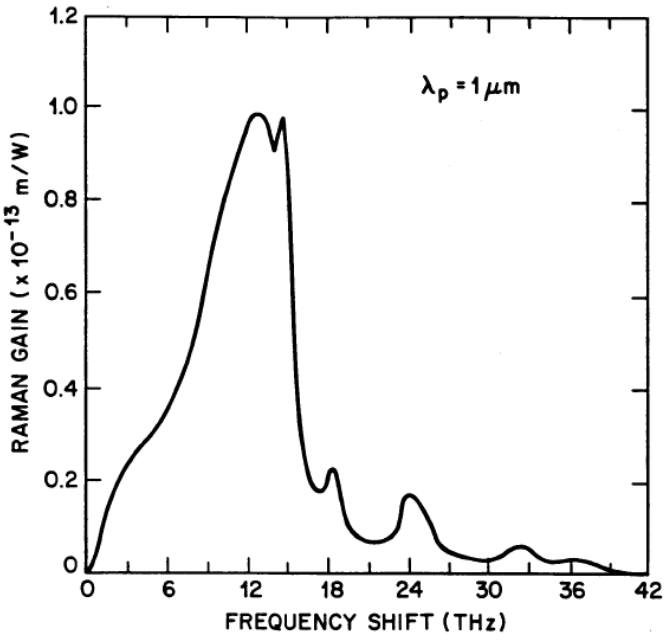

Figure 2.17: Typical Raman gain spectrum at pump wavelength 1 μm [6].

Now, we consider the threshold power: P_{th} for SRS. It describes the critical level of input pump power to generate Stokes wave. The mathematical definition is given as follow:

$$g_R P_{th} L_{eff} / A_{eff} \cong 16, \tag{2.4.3.1}$$

where g_R is the coefficient at the gain peak and L_{eff} is defined in Eq. (2.4.7). A typical P_{th} value within single mode fiber pumped at ~1550 nm wavelength, is about 600 mW, which is much higher than the power level in optical communication channel. Here, we use HNLF with high nonlinearity to decrease the threshold power and enhance Raman scattering.

In addition, when the intensity of Stokes waves satisfy the threshold condition, higher-order Raman Stokes waves also can be generated. In this situation, more pump lights can convert to long wavelengths Stoke waves and contribute to spectrum broadening. Multi-orders Stokes waves are presented in Figure 2.18, which is produced by a 1 kW pulse laser pump. It can be observed clearly that the intensity of higher-order Stokes lines decreases and the gain peaks are broadened gradually.

Since it can broaden the spectrum significantly, the SRS nonlinear effect plays a key role in SC generation.

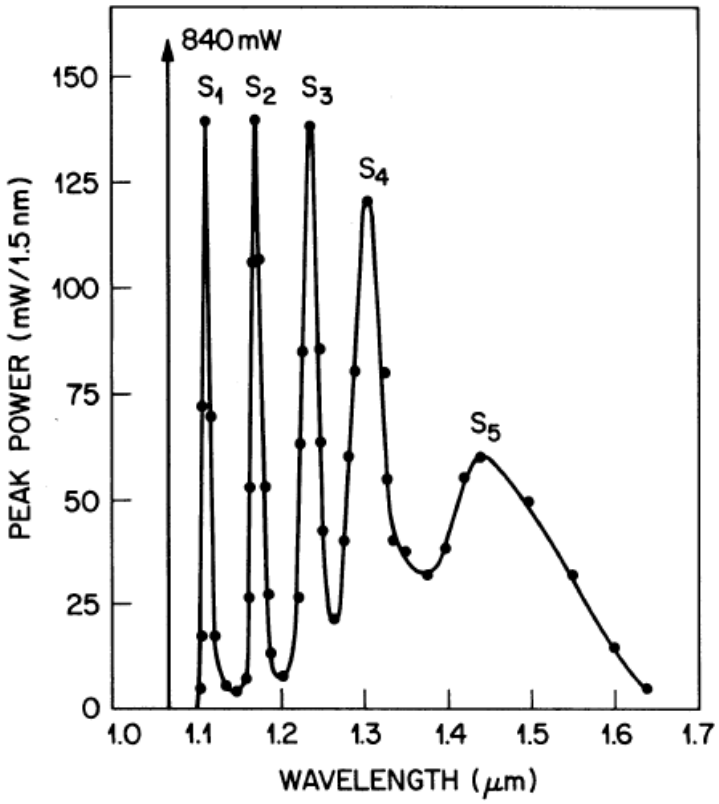

Figure 2.18: Cascaded Raman Stokes lines induced in the fiber [6].

Stimulated brillouin scattering (SBS) is also an inelastic scattering process. Like SRS, SBS also can induce frequency shift. However, the frequency shift between the new generated light and the pump in SBS is just about 10GHz, which is much narrower than in SRS. Furthermore, it propagates in the opposite direction compared to the pump. SBS effect occurs when pump intensity is sufficient. The corresponding threshold power P_{th} can be calculated by

$$g_B P_{th} L_{eff} / A_{eff} \cong 21, \qquad (2.4.3.2)$$

where g_B is the SBS gain co-efficient, and it is much larger than g_R. The SBS threshold is approximately 1 mW in single mode fiber. In general, the SBS effect is not considered in

supercontinuum generation due to limited bandwidth, only around ~10 GHz. Also, Brillouin gain is greatly reduced because of high threshold power. Furthermore, since the bandwidth of amplified spontaneous emission (ASE) is wider than 10 GHz, SBS effect is hard to be observed i our experiment.

2.4.4 Four-wave mixing (FWM) and modulation instability (MI)

Four-wave mixing (FWM) is also a nonlinear process when optical light propagates in optical fiber. It can be used to describe that the fourth optical wave is generated within an input involving three optical waves with different frequencies. The frequencies and wave-vectors of the input waves can be defined as $(\omega_1, \vec{k_1})$, $(\omega_2, \vec{k_2})$ and $(\omega_3, \vec{k_3})$. Then the frequency and wave-vector of the new generated wave is $(\omega_4, \vec{k_4})$, which can be written as :

$$\omega_4 = \omega_1 \pm \omega_2 \pm \omega_3, \tag{2.4.4.1}$$

$$\vec{k_4} = \vec{k_1} \pm \vec{k_2} \pm \vec{k_3} \tag{2.4.4.2}$$

The two equations illustrate the conservation of energy and momentum, which must be satisfied simultaneously. The wave-vector is correlated to frequency due to dispersion. Therefore, the FWM phenomenon requires certain condition: phase-matching. Here is a scheme that two photons with energies $\hbar\omega_1$ and $\hbar\omega_2$ generate another two photons with energies of $\hbar\omega_3$ and $\hbar\omega_4$ at frequencies ω_3 and ω_4 , respectively. Both energy and momentum conservation are satisfied as the following equation states:

$$\omega_4 = \omega_1 + \omega_2 - \omega_3 \tag{2.4.4.3}$$

$$\hbar\omega_1 + \hbar\omega_2 = \hbar\omega_3 + \hbar\omega_4 \tag{2.4.4.4}$$

This case can be simplified to match the phase-matching condition:

$$\omega_1 = \omega_2,$$

$$\omega_3 = \omega_1 + \Omega,$$

$$\text{and } \omega_4 = \omega_1 - \Omega,$$

where Ω is the frequency interval. In this case, the phase-matching condition contains three different parts: material dispersion Δk_M, waveguide dispersion Δk_W and nonlinear effects Δk_{NL}. They are defined, respectively, by

$$\Delta k = \Delta k_M + \Delta k_W + \Delta k_{NL} \tag{2.4.4.5}$$

$$\Delta k_M = [n_3\omega_3 + n_4\omega_4 - 2n_1\omega_1]/c \approx \beta_2\Omega^2, \tag{2.4.4.6}$$

$$\Delta k_W = [\Delta n_3\omega_3 + \Delta n_4\omega_4 - (\Delta n_1 + \Delta n_2)\omega_1]/c, \tag{2.4.4.7}$$

$$\Delta k_{NL} = \gamma(P_1 + P_2) = 2\gamma P_0, \tag{2.4.4.8}$$

where P_0 and γ are the pump power, nonlinear coefficient, respectively. The parameter: β_2 is GVD coefficient and it is related to dispersion parameter D, which is defined by

$$D = -\frac{2\pi c}{\lambda^2}\beta_2, \tag{2.4.4.9}$$

Generally, in single-mode fiber, contribution of material dispersion is much more than waveguide dispersion, except the region around zero-dispersion wavelength. To satisfy the phase-matching condition, the material dispersion contribution should be negative to compensate the contribution from nonlinear effects. Therefore, the pump light located in the anomalous dispersion region (D>0, $\beta_2 < 0$) of optical fiber is useful to generate FWM effect. The frequency spacing in phase-matching is at $\Omega = \pm\sqrt{\frac{2\gamma P_0}{|\beta_2|}}$.

Finally, modulation instability (MI) is discussed. MI describes a nonlinear phenomenon that spectral sidebands or pulse trains are generated from an optical wave due to fiber nonlinearity. In other words, the pump light can generate two symmetric spectrums through MI effect. The frequency spacing: Ω between the central frequency and sideband frequency is defined by: $\Omega = \pm\sqrt{\frac{2\gamma P_0}{|\beta_2|}}$, which is same as FWM. Figure 2.19 presents the spectrum with two sidebands at frequencies: $\omega_1 \pm \Omega$. This phase-matching condition is ensured by the nonlinear effects of SPM and MI effect contributes the sideband amplification. The frequency spacing is determined by the pump intensity. It can be up to 10 THz when hundreds Watts of pump power is used. Compared to MI effect, the spectrum broadening produced by FWM can be hundreds nanometers, which is illustrated in Figure 2.20. In addition, Raman Stokes line at ~13.2 THz from the pump wavelength can also be monitored in the optical spectrum. Similar to other nonlinear effects, FWM and MI also can contribute to broaden spectrum, especially in flat supercontinuum generation.

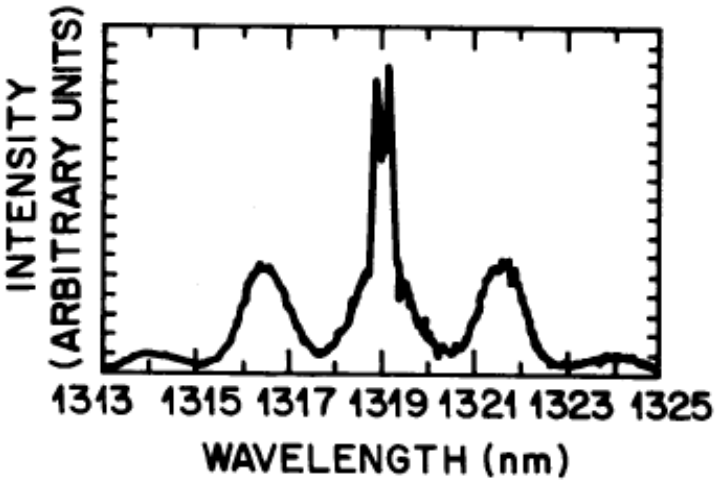

Figure 2.19: Spectrum with two side bands generated by MI effect [6].

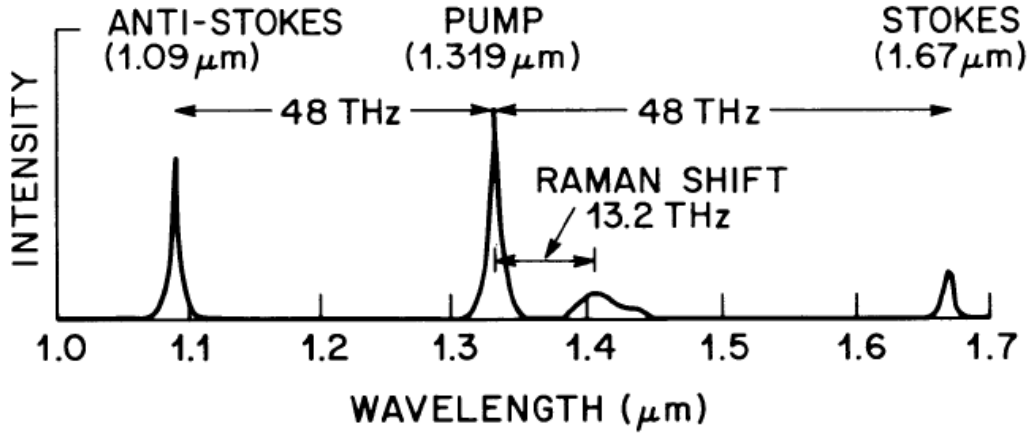

Figure 2.20: Stokes and anti-Stokes peaks generated by FWM effect [6].

CHAPTER 3 CW LASER PUMPED SC SOURCE

In this chapter, SC generation using CW pump laser will be demonstrated. Here, the evolution of SC as a function of pump power is shown and the internal physical mechanism is investigated. Finally, the output power and stability of the SC source will be further discussed.

3.1 Configuration of CW Lasers Pumped SC.

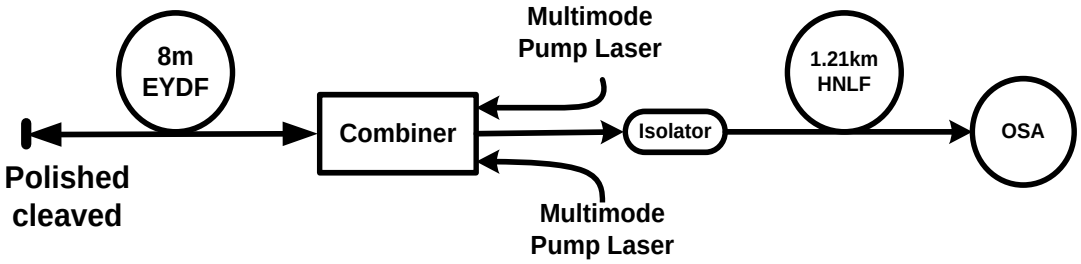

Figure 3.1: Setup of CW laser pumped SC generation.

The experimental setup above shows the whole configuration of the CW lasers pumped SC source. Note that the right end of the EYDF is polished and cleaved to construct a cavity, which can enhance the pump absorption efficiency. This design is different with the previous work [37]. The nonlinear effects occurred in the HNLF contribute to the broadband SC generation. The EYDF and HNLF have been analyzed in the previous chapter. Here, other optical devices are introduced.

1) Pump lasers:

Two 975 nm multimode CW lasers are used as low-cost pump lasers. The maximum output power is 6 W for each laser, which is sufficient to generate SC. In

particular, multimode CW pump laser is much cheaper than other pump sources, which is useful to reduce the cost of the SC source. Since overheat can result in laser wavelength shift easily and damage the laser eventually, heat sink, thermally conductive pyrolytic graphite sheet (PGS) and fan are used for thermal dissipation and improving the operation stability of pump laser. Detailed parameters of the multimode CW pump laser are given in Appendix B. The pump laser has a multimode fiber pigtail with 0.15 numerical apertures (NA), which is easy to couple with other optical components. In this work, two multimode CW pump lasers are coupled into an optical combiner.

2) Optical combiner and isolator

The optical combiner combines the CW multimode pump lasers and the double-cladding EYDF together. As seen in Figure 3.2, a (2+1)*1 multimode combiner is used to guide 975 nm pump light into the EYDF and transmits the 1550 nm light to HNLF. The operation wavelength range of signal and pump input ports are 1530-1560 nm and 900-1000 nm, respectively. Note that the pigtail of the signal port together with the output port is double cladding fiber (DCF). DCF is a special type of single-mode fiber (SMF) with lower refractive index coating outside than the fiber cladding. This design can enable the pump light to propagate in both fiber core and cladding regions, which makes the light loss as small as possible. The EYDF also has similar structural design. High power pump light could be coupled into the fiber core gradually, which can be absorbed and transferred efficiently. The detailed information about the optical combiner is given in Appendix C.

In addition, an optical isolator is used to maintain light transmission in the single direction and blocks the feedback in the opposite direction. The isolator used in our experimental setup can handle about 35 dBm of the feedback light.

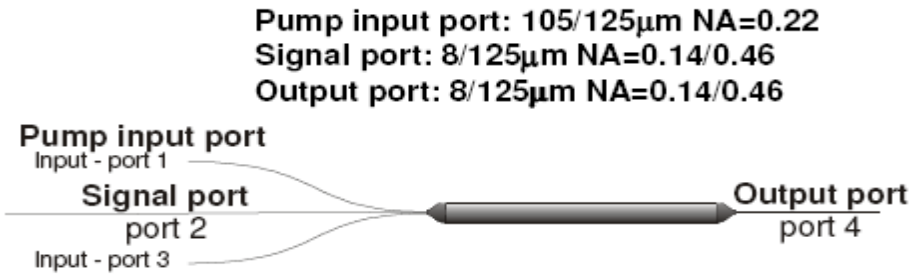

Figure 3.2: Diagram of the $(2+1)\times 1$ multimode combiner with three input ports and one output port.

3) Optical spectrum analyzer (OSA) and optical power meter

Two OSAs with different measurement scales are used to trace the SC output: ANDO AQ 6317B and Yokogawa AQ 6375, which can record the wavelength range 600-1750 nm and 1200-2400 nm, respectively. Both two OSAs can handle the input optical power: 20 dBm. Therefore, a high power attenuator is required to avoid OSA damage. The optical power is recorded by fiber optic power meter: ILX Lightwave FPM-8210H. The corresponding detecting range of wavelength and power level is from 850-1650 nm and from +30 dBm to -50 dBm, separately. Because of its wavelength limitation, the measured power level is lower than the actual power level of the SC source.

3.2 Optical Spectrum Evolution of SC

Firstly, we shall briefly introduce the ASE from the EYDF, which is converted from the pump light. Figure 3.3 shows the ASE spectrum from EYDF. When 1 W CW light pumps the EYDF, two clearly peaks are observed at: 1536 nm and 1543 nm. In addition, a small peak at 1564 nm also exists. All the three peaks are from the ASE and can operate in the HNLF to generate new frequencies. The SC spectrum at different pump power levels is shown in Figure 3.4. The values of pump power are set at 2, 4, 5, 6 and 7 W, separately. When the pump power is 2 W, a large optical peak is observed at 1543 nm. This peak results from the ASE in the EYDF and is broadened by SPM effect, which agrees with previous results [36, 37]. As the pump power is increased to 3 W, another apparent peak at 1660 nm is visible and is about 13.7 THz away from the ASE peak at 1543 nm. Typically, this peak is originated from the first-order Stokes line produced by SRS nonlinear effect in the HNLF and its broadness can also be attributed to SPM and MI [37]. Also, the peaks at 1754, 1829, 1893 and 1985 nm are the secondary and high-order Stokes line of SRS effect. Furthermore, three additional peaks are observed on the left sides of the 1543 nm peak at 1385, 1080 and 900 nm, which may be induced by the ASE of the EYDF and further amplified by the SPM effect in the long HNLF. If more pump power is provided, the long wavelength regions firstly tend to broaden and flatten because of SRS, MI and FWM nonlinear effects. When the pump power is 6W, both short and long wavelength components are broadened by the nonlinear effects of SRS, MI, FWM, SPM and XPM. Finally, the flat and ultra-broadband SC from 900 nm to more than 2000 nm is obtained and the bandwidth is more than 1100 nm. Note that once the ultra-broadband SC is formed, the spectrum is hardly to improve by adding pump power

further. It can be seen that the 7 W pumped SC spectrum is comparable to 6 W pumped SC. The whole optical spectrum is relatively flat and smooth except two main peaks at 1543 nm and 1655 nm, which is obviously resulted from ASE and first-order SRS, respectively. This SC is much wider than other results using multimode pump lasers [35-37]. This actually originates from two reasons. One is the high conversion efficiency of the doped fiber, while the other is that the single-line structure has little bandwidth limitation of the optical devices.

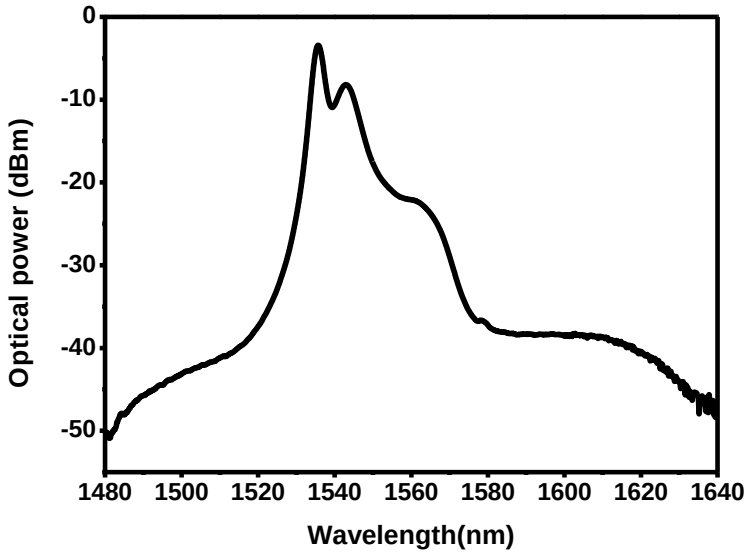

Figure 3.3: ASE spectrum from Er-Yb codoped fiber.

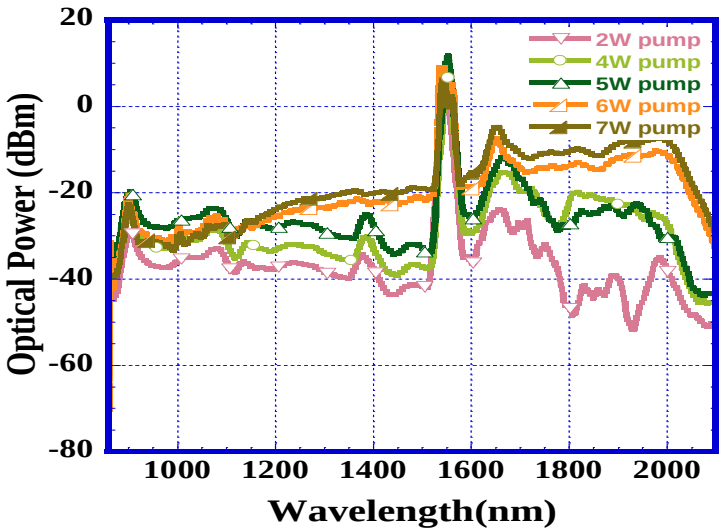

Figure 3.4: Measured broadband supercontinuum evolution with resolution 1 nm.

3.3 Analysis of Output Power

In this section, we will first analyze the power conversion from 975 nm pump light to 1550 nm ASE in EYDF. Here, PCE: power conversion efficiency is used to describe the evolution. The SC generation requires sufficient ASE power to induce numerous nonlinear effects in HNLF. High PCE is essential for a practical SC source.

Many factors including the doping element, doping concentration, the length of doped fiber, the connection loss as well as the pump power level can affect the PCE. In this work, 8 m long Er/Yb co-doped fiber from Fibercore Inc is used. Here, we concern the corresponding PCE at different pump power levels. For Erbium doped fiber (EDF), both directions can emit light: forward pump could maintain relative low noise figure, while high saturated output power can be obtained from backward pump [48]. Considering that the EYDF is comparable with EDF, the backward pump method is

preferred in our SC generation. The PCE evaluation needs to consider both outputs from two directions. In the experiment, the power meters are placed in two ends to measure the output power level, as shown in Figure 3.5. Related data is given in Table 3.1.

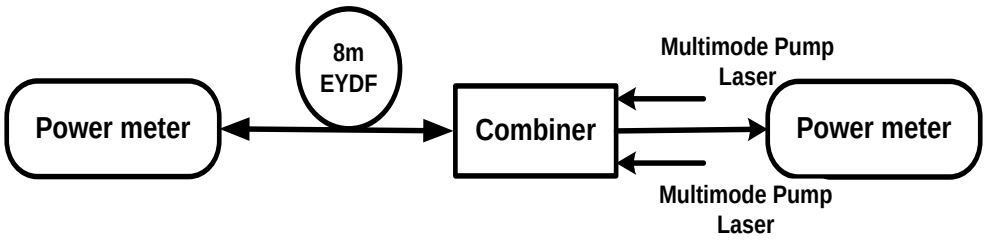

Figure 3.5: Measured PCE with two power meters.

Table 3.1: PCE parameters with respect to pump power. Both forward and backward conversion power are considered.

Forward (mW)	Backward (mW)	Pump power(W)	PCE	Forward (mW)	Backward (mW)	Pump power(W)	PCE
7.2	19.5	0.2	13.35%	181	310	1.2	40.92%
30	71	0.4	25.25%	219	377	1.4	42.57%
59	121	0.6	30%	270	441	1.6	44.44%
101	186	0.8	35.88%	314	503	1.8	45.39%
143	248	1	39.1%	338	591	2	46.45%

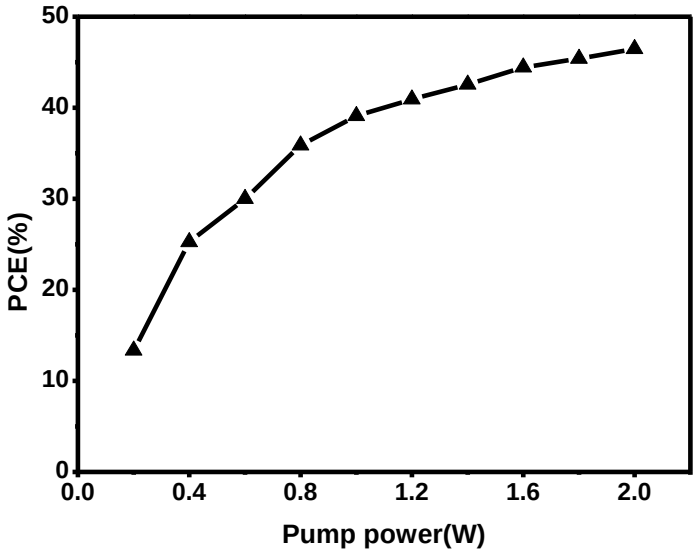

Figure 3.6: Evolution of PCE versus pump power.

It can be seen that the PCE is enhanced continually as the pump power increases. The PCE value is 46.45% at 2 W CW laser pumped. Because of the power meter limitation, the PCE is not characterized further.

After that, the output power of SC is discussed. Similarly, the output power of broadband source is measured at the end of HNLF. Figure 3.7 illustrates the total output power of this broadband source. It clearly shows that the SC intensity increases as a function of CW lasers pump power. We can observe that the output power of SC source has little change when the pump power increases from 4W to 5W. It can be explained by the extension of optical spectrum to the long wavelength region, which exceeds the scale of measurement device. This is consistent with the spectrum results. In addition, once the SC is obtained, the output power tends to increase slowly. Finally, ultra-broadband SC with around 200 mW output power is obtained. Considering the device limitation, the

total output power level should be higher than the measured results, especially when ultra-broadband SC is generated.

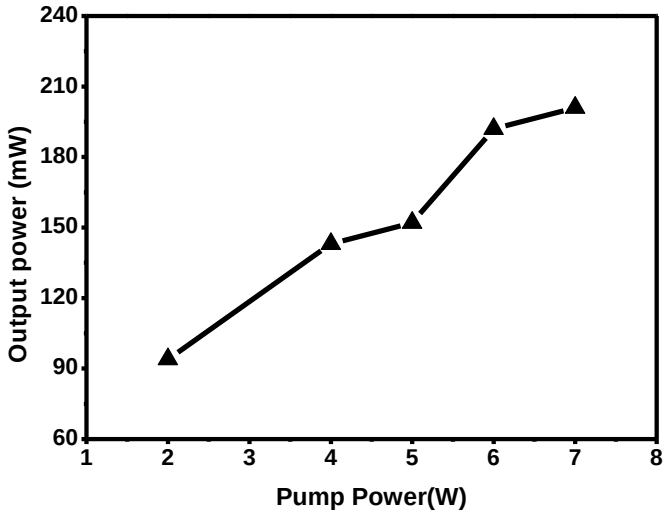

Figure 3.7: SC source output power as a function of pump power

3.4 Stability of Output Optical Spectrum

In this section, the long-term stability of the output the SC source is analyzed. While the pump power was set to be 6 W, the SC spectrums were recorded at five different moments: 0, 1, 3, 5 and 10 h, respectively. Figure 3.8 shows the measured results of obtained SCs. The resolutions of OSA are set at 1 nm for each measurement. The diagram shows clearly that no significant fluctuations are monitored in optical spectrum, as well as the power level. The spectrum is repeated deeply. Few fluctuations are caused by the instability of pump power, which may result from the temperature impact. If this issue is not considered, it can be said that the SC laser source is stable and practical.

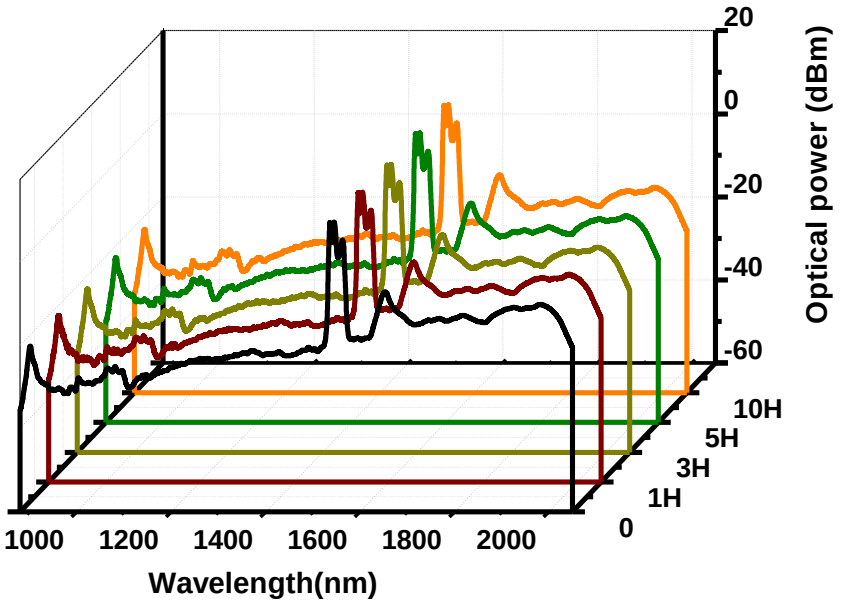

Figure 3.8: Measured SC output with the increase of operational time. The resolution of OSA is 1 nm.

CHAPTER 4 SUPERCONTINUUM GENERATION USING A SHORT PULSE FIBER LASER AND PHOTONIC CRYSTAL FIBER

Besides CW laser pumped SC, ultra-broadband SC source using short pulse trains and a new class of optical waveguide-PCF has attracted significant attention. The nonlinearity and group velocity dispersion of PCF can be engineered, which is supportive in SC generation. In this chapter, we will investigate the SC performance using a picosecond pulse laser and PCF with flat dispersion. The SC generation is investigated in terms of optical spectrum, output optical power, long term stability and RIN characteristics, respectively.

4.1 Optical Components Used in a Short-Pulse Laser Pumped SC

The experimental setup used in this work is shown in Figure 4.1, which includes a home-made passively figure-8 mode locked erbium-doped fiber laser (EDFL), an erbium-doped fiber amplifier (EDFA), and 13-m long PCF. A 2.4 picosecond $sech^2$-shaped ultra-short pulse is generated from the EDFL at center wavelength of 1554 nm. The temporal profile of the short pulse is characterized by using autocorrelator device, as shown in Figure 4.2. The repetition frequency and average output power are 3 MHz and 0.72 mW, separately. First, the pulse is amplified by the EDFA. The average power of amplified pulses can be up to about 101.5 mW and the corresponding peak power is estimated to be 14.1 kW. Note that the amplified pulses are not compressed further by using single mode fiber

(SMF), so the peak power may be lower due to the pulse broadening after transmission in the EDFA. Then, the amplified pulses are injected into a 13 m long PCF with flat dispersion, which is used as highly nonlinear medium to generate SC. The PCF has flat dispersion between two ZDWs, which are at around 1475 nm and 1650 nm, respectively.

The SC spectrum is recorded by two OSAs with different measurement regions: ANDO AQ 6317B (600-1700 nm) and Yokogawa AQ 6375 (1200-2400 nm). The resolutions of the two OSAs are set to 1nm. In addition, the RIN of SC source is characterized by using MXA Analyzer (N9020A 20Hz-26.5GHz) and digit-multimeter detector (N4371A) from Agilent Technology.

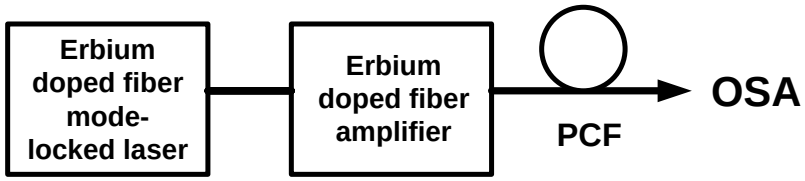

Figure 4.1: Experimental setup of a short-pulse laser pumped broadband source.

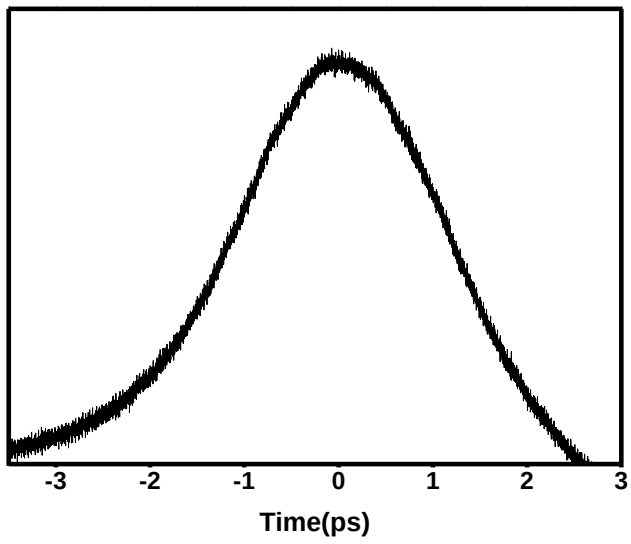

Figure 4.2: Intensity profile of short pulse generated from Erbium doped fiber laser.

4.2 Optical Spectrum Evolution of Supercontinuum Generation Using a Picosecond Pulses Laser and PCF

The detailed evolution of the SC spectrum by using a picosecond pulse pump laser is shown in Figure 4.3. The SC generations are investigated as a function of pump power. When the average pump power is 2 mW, a relatively narrow optical spectrum with a peak around 1554 nm is observed. This can be attributed to the amplified spontaneous emission (ASE) noise from the EDFA in the setup. As the injection power increases, the optical spectrum is broadened gradually on both sides of 1554 nm, which is clearly caused by self-phase modulation (SPM) effect. By further increase of the injection power, stimulated Raman scattering (SRS) induces spectrum broadening in long wavelengths firstly. With higher pump power, the optical spectrum in the shorter wavelength range is also broadened notably, which is mainly caused by four wave mixing (FWM). When the injection power is 52.3 mW, a relative flat and broadband SC is generated. The total SC bandwidth and output power are 720 nm and 13.2 dBm. The optical spectrum is smooth and presents few fine structures. Eventually, the flat and ultra-broadband source from 1200 nm to 1920 nm is obtained when the pump power is 101.5mW. The SC source output power is 15.5 dBm, while the whole spectrum flatness is about 11dB. Particularly, the original injection pump peak almost disappears in the obtained SC, which is much different from the previous reports of SC generations [7]. In Figure 4.3 inset, SC obtained by NKT is also shown using the similar technologies [2]. Compared to NKT, our obtained SC source is much flatter and wider. It may be explained by the fact that the length of the PCF, the peak power and pump wavelength of the short pulse are optimized.

In previous reports, the SC obtained by using a femotsecond pump laser is mostly explained by SPM, while spectral broadening by picosecond or nanosecond pump is dominated by SRS and FWM [7]. It is shown that our SC generation is mainly thanks to SPM, SRS and FWM corresponding to different regions of spectral broadening. Additionally, since this type of PCF has two ZDWs and flattened dispersion between them, more modulation instability (MI) together with FWM can be obtained to flatten the SC. Therefore, the flat and broadband SC as shown in Figure 4.3 is attributed to more FWM and MI compared to CW laser pumped SC.

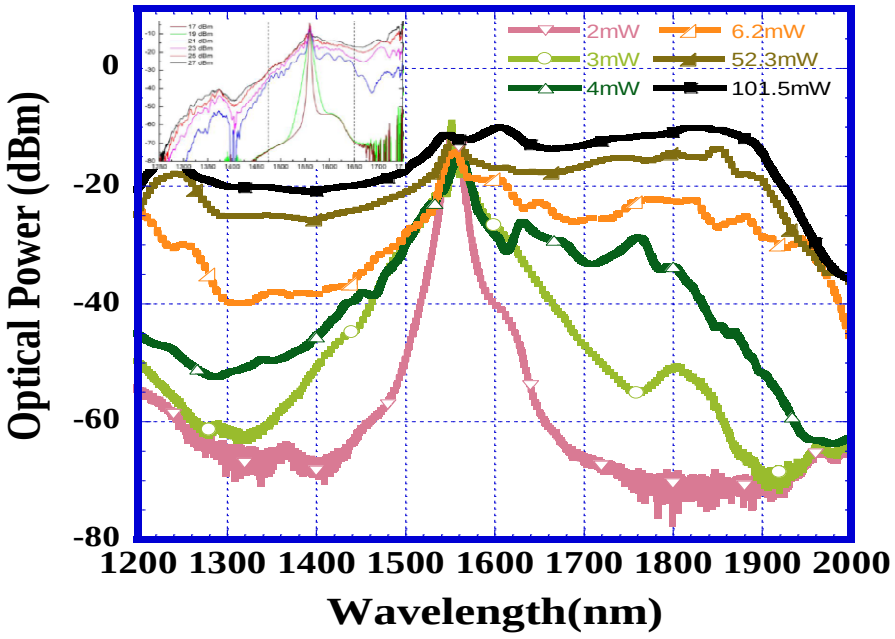

Figure 4.3: Measured optical spectrum with resolution of 1 nm at different injection power to PCF. The NKT results are shown in the inset [2].

4.3 Output Power Evaluation of Supercontinuum Generation

In this section, we focus on the output power of the broadband SC source. In Table 4.1, corresponding optical power is listed.

Table 4.1: Output power evolution of SC source.

EDFA / POWER LEVEL	0.03	0.05	0.06	0.08	0.5	0.6	0.7	0.8	0.9
Pulse(mW)	0.72	0.72	0.72	0.72	0.72	0.72	0.72	0.72	0.72
Amplified pulse(mW)	2	3	4	6.2	52.3	70	81.6	92	101.5
Pulse Peak power (kW)	0.278	0.417	0.556	0.861	7.264	9.722	11.33	12.78	14.1
SC output(mW)	0.3	0.5	1	1.5	20.9	23.5	27.9	31	35.5

From the list above, we can see that the output power of SC source increases continuously with the pulse power amplified. When the flat and ultra-broadband SC is achieved, the output power is more than 30 mW. In this system, the maximum optical power and the optical power spectral density of SC are 35.5 mW and -13 dBm/nm, separately, when the pump peak power is 14.1 kW. It seems that the output power and the spectrum flatness will be improved further with boosting the peak power of the short pulse.

4.4 Stability of Supercontinuum Generation

In this section, the long term stability of SC is investigated. The spectrum was recorded every 1 hour for 5 hours while the pump power and peak power of short pulse were maintained at 101.5 mW and 14.1 kW, respectively. The spectrum results are shown in Figure 4.4. The flatness and bandwidth of spectrum are repeated successfully. No

significant fluctuations are observed in the spectrum, which reveals that the SC source output is stable. It demonstrates that our SC source is stable and practical.

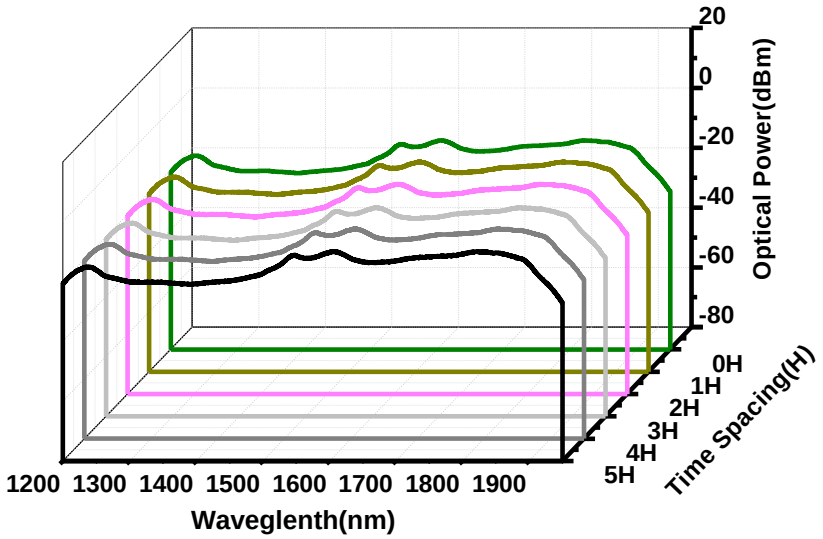

Figure 4.4: Optical spectrum of the SC recorded for 5h with spacing 1h at the pump power of 101.5mW. The resolution is maintained at 1 nm.

Additionally, we use a 700M photo-detector and a digital oscilloscope to characterize the SC source in temporal domain, as given in Figure 4.5. It shows that the SC laser source exists in the form of short pulse trains with repetition rate 3.15 MHz. This is comparable with the pump pulse from the figure-8 laser, which is potential to use for short pulse generation and others applications.

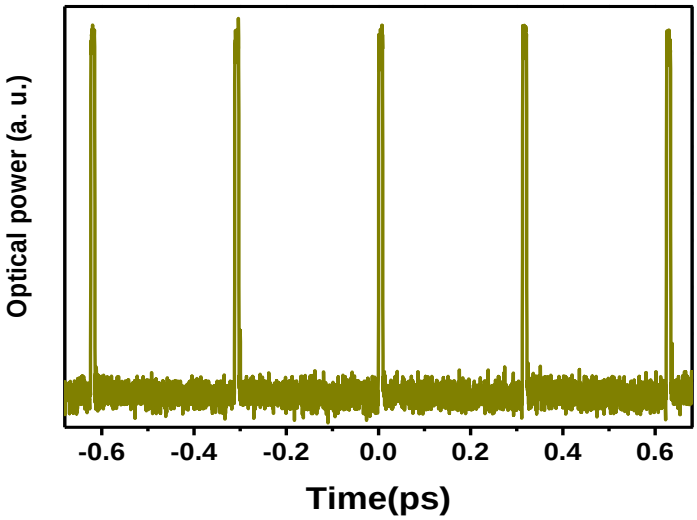

Figure 4.5: Optical power versus time for the short-pulse laser pumped SC output.

4.5 Relative Intensity Noise (RIN) Characteristics of the Broadband Source.

Here, we also measured the RIN characteristics of the supercontinuum source. The detailed RIN information from 10 to 100 MHz is shown in Figure 4.6. First, the RIN value of figure-8 fiber laser is measured as a reference. The RIN value is -93.8 dBc/Hz. Then the RINs of broadband source are determined. At the beginning, the RIN value is very high. The high RIN level results from the nonlinearity and dispersion behaviors at the beginning of spectrum broadening. As the spectrum is broadened and flattened, the RIN decreases progressively. Finally, the RIN of the flat and broadband SC is comparable to the pump pulse laser source and even can be lower than pump laser. At 101.5 mW pulse pumped SC source, the corresponding RIN is -96dBc/Hz, which is 2dBc/Hz lower than the Er-doped fiber laser. The RIN of the broadband source is well suppressed instead of amplification in SC generation.

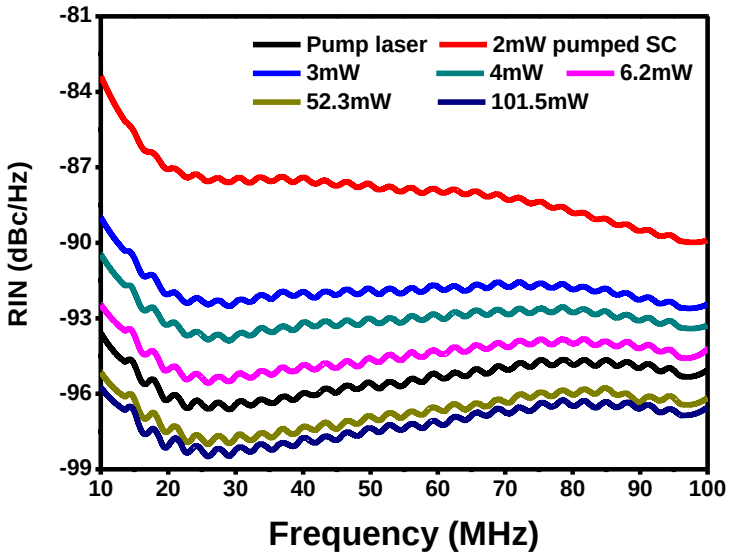

Figure 4.6: Comparison of RIN characteristics of the SC source and the pump laser.

4.6 Comparison of the Supercontinuum Generations Using CW-HNLF and Pulse-PCF

Firstly, ultra-broadband SC laser source using CW laser pumped and HNLF are obtained successfully. The bandwidth is more than 1100 nm, spanning from 900 nm to more than 2000 nm, which is much wider than other reports using similar technologies. Particularly, the ultra-broadband SC source using multimode pump lasers maintains low cost. The optical spectrum is almost flat and smooth except for two apparent peaks. And, the output optical power is up to hundreds milliWatt. The single-line structure is useful to broaden the optical spectrum with minimum bandwidth limitation. Secondly, a broadband and flat SC light source has been obtained by using ps pulse trains and PCF with flat dispersion. The optical spectrum of SC source is from 1200 to 1920 nm. The spectrum flatness of the broadband source is better than 11dB. No obvious pump peak is observed. The high

flatness and wide bandwidth are obtained simultaneously, which is much better than other SC generations using similar technologies. In particular, the pump wavelength is in the optical communication window, which is critical in practical commercial application. In short, our flat broadband SC source is compact, stable, and free from spectral fine structure.

Compared with SC based CW and HNLF, the PCF-generated SC is very flat and without the residual pump peak, which is practical in commercial applications. The CW laser pumped SC laser source has higher output power and maintains low system cost, which is also important for commercial products.

CHAPTER 5 CONCLUSIONS

5.1 Summary

In this section, conclusions and future work are summarized. Two different SC sources: CW laser pumped HNLF and ultra-short pulse laser pumped PCF, have been investigated in this thesis, because of their numerous applications such as in frequency metrology, OCT, as well as DWDM, etc.

Firstly, we have demonstrated an ultra-broadband SC source using CW laser pumped HNLF, which is mainly composed of two low-cost multimode 975 nm CW pump lasers, 8 m long EYDF and 1.21 km HNLF. The 975 nm pump light is absorbed firstly by EYDF and converted to 1543 nm ASE seed light, which is nearby the ZDW of HNLF. Then the light experiences intense spectral broadening by using nonlinear effects, such as SPM, XPM, SRS, MI and FWM. The role of nonlinear effects in SC generation has been discussed, which provides detailed evidences to understand the internal physic mechanism. The SC spectrum from 900 to more than 2000 nm has been obtained successfully. It is seen that apart from the pump peak and first-order SRS peak, the remaining spectrum is relative flat. The total output optical power is more than 200 mW. The stability of the optical spectrum and power level is well maintained after several hours of operation. Additionally, this SC laser source is considered low cost broadband source, which is useful for commercial applications.

Secondly, a broadband fiber-based SC laser source covering from 1200 to1920 nm has been generated by using picosecond pulse laser pumped PCF with flat dispersion. This broadband source consists of a home-made figure-8 fiber laser, an EDFA and 13m

long PCF with flat dispersion between two ZDWs. For this SC generation, the pump peak is absorbed completely and almost disappears in the final optical spectrum. The optical spectrum without any obvious peaks shows smooth and fine structure free characteristics. The spectral bandwidth is more than 700 nm while the spectrum flatness is better than 11dB, which is originated from SRS, FWM and MI. The total optical output power and power spectral density are 35.5 mW and -13 dBm/nm, respectively. Similarly, the long term stability of this SC source is well maintained.

Above all, the HNLF and PCF are considered as high nonlinear media in two kinds of configurations, separately. The detailed investigation in this thesis is useful to understand the highly complex process in SC generation. In addition, both of the two SC laser sources have the potential to be commercial products.

5.2 Future Work

Future research will focus on the high quality SC with high power spectral density and spectrum flatness, which can be widely commercialized.

First, in the single-line CW laser pumped structure much ASE power in the forward direction is not used in SC generation. It has been demonstrated that all the ASE from both of forward and backward can be used in SC generation. Considering the bandwidth of optical device, free space coupler is a good choice in proper design. Then high quality SC with ultra-broadband width and high output power can be obtained in future work.

Second, the length of the Er/Yb co-doped fiber and HNLF can be optimized further, which is useful to improve the efficiency of SC generation.

Third, the peak power of pulse trains and the length of PCF are key parameters to generate SC source. High peak power pulse can induce sufficient nonlinear effects to yield broadband SC. We believe that high quality SC source can be generated by using short pulse laser with higher peak power. Besides, the optimized dispersion properties and length of PCF also can broaden and flatten the SC spectrum further.

Fourth, the applications of SC are considered. High quality SCs can be used in ultra-short pulse generation and OCT.

REFERENCES

[1] I. Hartl, X. D. Li, C. Chudoba, R. K. Ghanta, T. H. Ko, J. G. Fujimoto, J. K. Ranka and R. S. Windeler, "Ultrahigh-resolution optical coherence tomography using continuum generation in an air-silica microstructure optical fiber", Optics Letters, Vol. 26, No. 9, pp. 608-610, 2001.

[2] K. Hansen and R. Kristiansen, "Supercontinuum Generation in Photonic Crystal Fibers," Application note on Crystal Fiber A/S website: http://www.crystal-fibre.com/support/Supercontinuum%20-%20General.pdf

[3] S. Smirnov, J. Ania-Castanon, T. Ellingham, S. Kobtsev, S. Kukarin, and S. Turitsyn, "Optical spectral broadening and supercontinuum generation in telecom applications", Optical Fiber Technology, Vol. 12, pp. 122-147, 2006.

[4] T. Kuri, T. Nakasyotani, H. Toda and K. Kitayama, "Characterizations of supercontinuum light source for WDM millimeter-wave-band radio-on-fiber systems," Photonics Tech. Lett, Vol. 17, pp. 1274-1276, 2005.

[5] J. Dudley and S. Coen, "Cohence properties of supercontinuum spectra generated in photonic crystal and tapered optical fibers," Optics Letters, Vol. 27, NO. 13, pp. 1180-1182, 2002.

[6] G. Agrawal, "Nonlinear Fiber Optics," 3rd Edition, Academic Press, San Diego, CA, 2001.

[7] J. M. Dudley, G. Genty, and S. Coen, "Supercontinuum generation in photonic crystal fiber," Reviews of Modern Physics, Vol. 78, pp. 1135-1184, 2006.

[8] R. R. Alfano and S. L. Shapiro, "Emission in the region 4000 to 7000 Å via four-photon coupling in glass," Phys. Rev. Lett., Vol. 24, pp. 584-587, 1970.

[9] J. K. Ranka, R. S. Windeler and A. J. Stentz, "Visible continuum generation in air-silica microstructure optical fibers with anomalous dispersion at 800nm," Opt. Lett., Vol. 25, pp. 25-27, 2000.

[10] J. Herrmann, U. Griebner, N. Zhavoronkov, A. Husakou, D. Nickel, J. C. Knight, W. J. Wadsworth, P. S. Russel, and G. Korn, "Experimental evidence for supercontinuum generation by fission of higher-order solitons in photonic fibers," Phys. Rev. Lett., Vol. 88(17), No. 173901, 2002.

[11] B. R. Washburn, S. E. Ralph, P. A. Lacourt, J. M. Dudley, W. T. Rhodes, R. S. Windeler, and S. Coen, "Tunable near-infrared femtosecond soliton generation in photonic crystal fibers," Electron. Lett., Vol. 37, pp. 1510-1512, 2001.

[12] B. R. Washburn, S. E. Ralph, and R. S. Windeler, "Ultrashort pulse propagation in air-silica microstructure fiber," Opt. Express, Vol. 10, pp. 575-580, 2002.

[13] G. Genty, M lehtonen, H. Ludvigsen, J. Broeng, and M. Kaivola, "Spectral broadening of femtosecond pulses into continuum radiation in microstructured fibers," Opt. Express, Vol. 10, pp. 1083-1098, 2002.

[14] A. Ortigosa-Blanch, J. C. Knight, and P. St. J. Russell, "Pulse breaking and supercontinuum generation with 200-fs pump pulses in photonic crystal fiber," J. Opt. Soc. Am. B., Vol. 19, pp. 2567-2572, 2002.

[15] J. H. V. Price, W. Belardi, T. M. monro, A. Malinowski, A. Piper, and D. J. Richardson, "Soliton transmission and supercontinuum generation in holey fiber using a diode pumped ytterbium fiber source," Opt. Express, Vol. 10, pp. 382-387, 2002.

[16] W. H. Reeves, D. V. Skryabin, F. Biancalana, J. C. Knight, P. St. J. Russel, F. G. Omenetto, A. Efimov, and A. J. Taylor, "Transformation and control of ultra-short pulses in dispersion-engineered photonic crystal fibers," Nature, Vol. 424, pp. 511-515, 2003.

[17] I. Cristiani, R. Tediosi, L. Tartara, and V. Degiorgio, "Dispersive wave generation by solitons in microstructured optical fibers," Opt. Express, Vol. 12, pp. 124-135, 2004.

[18] G. Genty, M. Lehtonen, and H. Ludvigsen, "Effects of cross-phase modulation on supercontinuum generated in microstructured fibers with sub-30 fs pulses," Opt. Express, Vol. 12, pp.4614-4624, 2004.

[19] S. Coen, A. H. L. Chau, R. Leonhardt, J. D. Harvey, J. C. Knight, W. j. Wadsworth, and P. St. J. Russell, "White-light supercontinuum generation with 60-ps pump pulses in a photonic crystal fiber," Opt. Lett., Vol. 26, pp. 1356-1358, 2001.

[20] L. Provino, J. M. Dudley, H. Maillotte, N. Grossard, R. S. Windeler, and B. J. Eggleton, "Compact broadband continuum source based on microchip laser pumped microstructured fiber," Electron. Lett., Vol. 37, pp. 558-560, 2001.

[21] S. Coen, A. H. L. Chau, R. Leonhardt, J. D. Harvey, J. C. Knight, W. j. Wadsworth, and P. St. J. Russell, "Supercontinuum generation by stimulated Raman scattering and parametric four-wave mixing in photonic crystal fiber," J. Opt. Soc. Am. B., Vol. 19, pp. 753-764, 2002.

[22] P. A. Champert, S. V. Popov, M. A. Solodyankin, and J. R. Taylor, "Multiwatt average power continua generation in holey fibers pumped by kilowatt peak power seeded ytterbium fiber amplifer," Appl. Phys. Lett., Vol. 81, pp.2157-2159, 2002.

[23] A. B. Rulkov, M. Y. Vyatkin, S. V. Popov, J. R. Taylor, and V. P. Gapontsev, "high brightness picoseconds all-fiber generation in 525-1800 nm range with picoseconds Yb pumping," Opt. Express, Vol. 13, pp. 377-381, 2005.

[24] A. Boucon, D. Alasia, J. Beugnot, G. Melin, S. Lempereur, A. Fleureau, H. Maillotte, J. Dudley, and T. Sylvestre, "Supercontinuum generation from 1.35 to 1.7 μm by nanosecond pumping near the second zero- dispersion wavelength of a microstructured fiber," IEEE Photonics Technol. Lett., Vol. 20, pp. 842-844, 2008.

[25] M. H. Alexander, "Pulse preserving flat-top supercontinuum generation in all-normal dispersion photonic crystal fibers," J. Opt. Soc. Am. B., Vol. 27, No. 3, pp. 550-559, 2010.

[26] K. L. Corwin, N. R. Newbury, J. M. Dudley, S. Coen, S. A. Diddams, K. Weber, and R. S. Windeler, "Fundamental Noise limitation to Supercontinuum Generation in Microstructure Fiber," Physical Review letters, Vol. 90, No. 11, pp. 113904, 2003.

[27] K. K. Chow, Y. Takushima, C. Lin, C. Shu, and A. Bjarklev, " Flat super-continuum generation based on normal dispersion nonlinear photonic crystal fiber," Electron Lett, Vol. 42, pp. 989-991, 2006.

[28] J. J. Miret, E. Silvestre, and P. Andres, "Octave-spanning ultraflat supercontinuum with soft-glass photonic crystal fibers," Opt. Express, Vol. 17, No. 11, pp. 9197-9203, 2009.

[29] J. Cascante-Vindas, S. Torrres-peiro, A. Diez, and M. V. Andres, "Supercontinuum generation in highly Ge-doped core Y-shaped microstructured optical fiber," Appl Phys B., Vol. 98, pp. 371-376, 2010.

[30] S. J. Im, A. Husakou, and J. Herrmann, "High-power soliton-induced supercontinuum generation and tunable sub-10-fs VUV pulses from kagome-lattice HC-PCFs" Opt. Express, Vol. 18, No. 6, pp. 5637-5374, 2010.

[31] A. Shirakawa, J. Ota, M. Musha, K. Ueda, J. R. Folkenberg, and J. Broeng, "Large-mode-area erbium-ytterbium-doped photonic-crystal fiber amplifer for high energy femtosecon pulse at 1.55μm," Opt. Express, Vol. 13, pp. 1221-1227, 2005.

[32] A. V. Avdokhin, S. V. Popov, and J. R. Taylor, "Continuous-wave, high-power, Raman continuum generation in holey fibers," Opt. Lett., Vol. 28, pp. 1353-1355, 2003.

[33] A. K. Abeeluck, C. Headley, and C. G. Jørgensen, "High-power supercontinuum generation in highly nonlinear dispersion-shifted fibers by use of a continuous-wave Raman fiber laser," Opt. let., Vol. 29, pp. 2163-2165, 2004.

[34] S. Li, A. B. Ruffin, and D. V. Kuksenkov, "Efficient generation of CW supercontinuum in optical fiber pumped by ASE light," Optical Fiber Communication Conference (OFC) 2006, paper OW132, 2006.

[35] J. Lee, Y. Takushima, and K. Kikuchi, "Continuous wave supercontinuum laser based on an erbium-doped fiber ring cavity incorporating a highly nonlinear optical fiber," Optics Lett., Vol. 30, pp. 2599-2601, 2005.

[36] Y. Song, "Ultra wideband CW pumped optical supercontinuum source", Dissertation, Master of Applied Science, Concordia University, 2007.

[37] Z. Jiao, "Broadband optical supercontinuum generation using low-cost multimode 975-nm pump lasers", Dissertation, Master of Applied Science, Concordia University, 2008.

[38] http://www.rp-photonics.com/erbium_doped_gain_media.html.

[39] G. Sefler, W. Mack, G. Valley, and T. Rose, "Secondary energy transfer and non-participatory Yb^{3+} ions in $Er^{3+}-Yb^{3+}$ high-power amplifier fibers," J. Opt. Soc. Am. B, Vol. 21, NO. 10, pp. 1740-1747, 2004.

[40] http://www.nufern.com/specsheets/eydf_7130.pdf, data sheet from Nufern.

[41] http://www.fibercore.com/CP1500.pdf.

[42] M. Hirano, "Highly nonlinear fibers and their applications," Optical Communications R&D Laboratories, Sumitomo Electric Industries, Ltd., NMIJ-BIPM Joint Workshop, 2007.

[43] O. Toshiaki, H. Masaaki, N. Tetsuya, and O. Masashi, "Highly-nonlinear optical fibers and their applications," SEI Technical Review, NO. 62, pp. 34-40, 2006.

[44] J. Nicholson, A. Abeeluck, C. Headley, M. Yan and C. Jørgensen, "Pulsed and continuous-wave supercontinuum generation in highly nonlinear, dispersion-shifted fibers," Applied Physics B, Vol. 77, pp. 211-218, 2003.

[45] http://www.nktphotonics.com/files/files/NL-1550-POS-1-100409.pdf.

[46] G. Agrawal, "Fiber-optic communication systems," 3rd edition, New York: Wiley-Interscience, 2002.

[47] http://www.rp-photonics.com/self_phase_modulation.html

[48] C. Giles and E. Desurvire, "Modelling Erbium-Doped Fiber Amplifiers", Journal of Lightwave Technology Letters, Vol. 9, No. 2, pp. 271-283, 1991.

APPENDIX A DATASHEET OF THE PHOTONIC CRYSTAL FIBER

NKT Photonics
the power of light

Crystal Fibre • *aero*LASE • Koheras • SuperK

Highly Nonlinear

NL-1550-POS-1

Nonlinear Photonic Crystal Fiber

- Small mode field area
- High nonlinear coefficient
- Flat positive dispersion

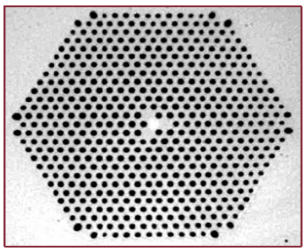

Photonic crystal fibers use a microstructured cladding region with air holes to guide light in a pure silica core, giving rise to novel functionalities.

This highly nonlinear photonic crystal fiber benefits from a special core design to obtain a very flat dispersion curve over the telecom wavelength range.

The slightly positive dispersion values of this fiber support soliton propagation and makes it attractive for applications such as supercontinuum generation and optical parametric amplification (OPA). Other fiber versions with near zero or negative dispersion values are also available.

The fiber is available spliced to standard single mode fiber.

Applications
- Supercontinuum generation
- Optical parametric amplification

Physical properties	
Material	Pure Silica
Cladding diameter	128 ± 5 µm
Coating diameter	250 ± 10 µm
Coating material, single layer	Acrylate
Core diameter*	2.1 ± 0.3 µm

*Triangular core, average diameter

Optical properties	
Dispersion @ 1480-1620 nm	>0.5 ps/nm/km
Dispersion @ 1480-1620 nm	<1.5 ps/nm/km
Attenuation @ 1510-1620 nm	<9 dB/km
Mode field diameter @ 1550 nm	2.8 ± 0.5 µm
Numerical aperture @ 1550 nm	0.40 ± 0.05
Nonlinear coefficient @ 1550 nm	~11 $(Wkm)^{-1}$
Splicing loss @ 1550 nm*	<0.5 dB

*Total splicing loss for splicing to standard fiber via an intermediate fiber

Typical spectral attenuation

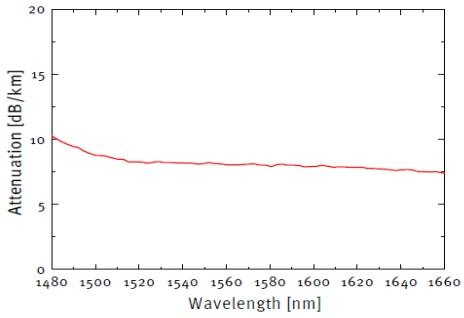

Typical dispersion

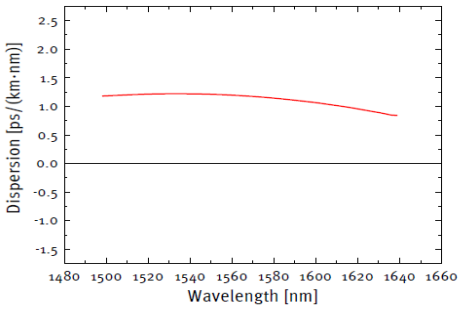

NL-1550-POS-1-100409

NKT Photonics A/S (Headquarters)
Blokken 84 • 3460 Birkerød • Denmark
Phone: +45 4348 3900
Fax: +45 4348 3901
www.nktphotonics.com

NKT Photonics GmbH
Schanzenstrasse 39 • Bldg D9-D13
51063 Cologne • Germany
Phone: +49 221 99511-0
Fax: +49 221 99511-650

NKT Photonics Inc.
1400 Campus Drive West • Morganville
NJ 07751 • USA
Phone: +1 732 972 9937
Fax: +1 732 414 4094

APPENDIX B DATASHEET OF THE PUMP LASER

EM4

6W 975nm 2 Pin Multimode Pump Laser

Features

- 0.15 or 0.22NA 105µm core multimode fiber pigtail
- Uncooled
- Laser welded and epoxy free
- Hermetically sealed
- RoHS compliant
- Qualified high reliability build structure

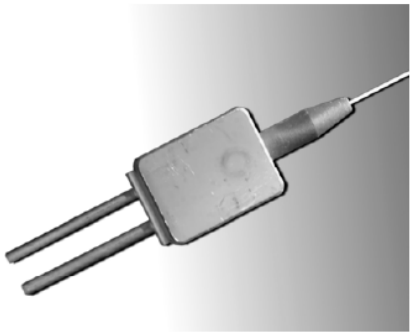

Applications

- Fiber lasers
- Yb laser pumping
- Marking
- Material processing
- Printing

General Description

The EM4 low cost RoHS compliant multimode pump is designed for pumping fiber lasers. It provides 6W of light fiber coupled into a 105µm core multimode fiber with numerical aperture of 0.15 or 0.22. The pump laser chip is built into a 2 pin package. The design and build of the module fulfills the requirements of Telcordia GR-468 and uses EM4 proven manufacturing processes.

Ordering Information

Part Number	λ_C [nm]	Fiber NA
EM304	975	0.15
EM305	975	0.22

Absolute Maximum Ratings

Stresses beyond those listed under "Absolute Maximum Ratings" may cause permanent damage to the device. These are stress ratings only and operation of the device at these or conditions beyond these are not implied. Exposure to absolute maximum ratings for extended periods of time may affect device reliability.

Parameter	Sym	Condition	Min	Max	Unit
Storage Temperature	T_{STG}		-40	85	°C
Operating Case Temperature	T_{OP}		-20	70	°C
Laser Forward Current	I_F			11	A
Laser Reverse Voltage	V_R			2	V
Lead Soldering Time				10	s
Lead Soldering temperature				250	°C
ESD		HBM		500	V

Optical And Electrical Characteristics

T_C=25°C unless otherwise specified, good thermal interface

Parameter	Sym	Condition	Min	Typ.	Max	Unit
Center Wavelength	λ_C	$I=I_{OP}$-1	965	975	985	nm
Operating Current	I_{OP}	$P=P_{OP}$			8	A
Operating Voltage	V_{OP}	$I=I_{OP}$			2.2	V
Output Power	P_{OP}		6			W
Threshold Current	I_{TH}			0.4	0.6	A

Optical And Electrical Characteristics (continued)

T_C=25°C unless otherwise specified.

Parameter	Sym.	Condition	Min	Typ.	Max	Unit
Wavelength Drift vs. T_C	$\delta\lambda/\delta T_C$			0.3		nm/°C
Spectral Width	$\Delta\lambda$	-17dB down from peak		6		nm
Operating Case Temperature	T_C		0		45	°C

Fiber Specification

Parameter	Typ.	Unit
Fiber Type	Step Index	-
Numerical Aperture	0.15 or 0.22	-
Core Diameter	105	µm
Outer Diameter	125	µm
Buffer Diameter	250	µm
Jacket Material	PVDF	-
Jacket Diameter	900	µm
Jacket length from end of boot	85±10	mm
Pigtail Length Min	1	m

Pinning

Pin	Description
1	Laser Anode (+)
2	Laser Cathode (-)

Mechanical Drawing

All units in mm

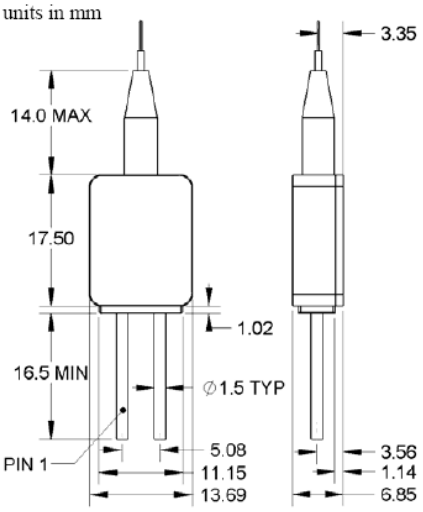

Typical Operating Characteristics

T_C=25°C

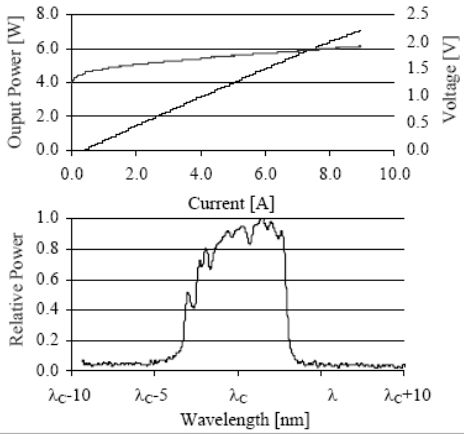

The component complies with all applicable portions of 21 CFR 1040.10, 21 CFR 1010.2 and 21 CFR 1010.3. Since this is a component, it does not comply with all of the requirements contained in 21 CFR 1040.10 and 21 CFR 1040.11 for complete laser products.

For pricing and delivery information, please contact EM4 inc. direct at +1 781 275 75 01, sales@em4inc.com or any of the representatives listed at www.em4inc.com.

APPENDIX C DATASHEET OF THE PUMP COMBINER

PRODUCT SPECIFICATIONS

PART ID: MMC02112A60

Avensys Tech

(2+1) x 1 Multimode Combiner
(105/125 µm NA=0.22 + 8/125 µm NA=0.14/0.46 –> 8/125 µm NA=0.14/0.46)

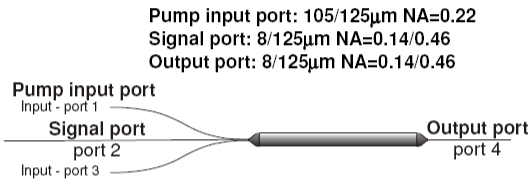

Environmental and Mechanical Specifications

Power handling	7 W per pump port
Port configuration	(2+1) x 1
Maximum Overall length (L)	65 mm
Diameter (Ø)	3.5 mm
Storage Temperature	-40/ +70 °c
Max Operating temperature	+60°c at the hottest point
Fiber types	
Ports 1 and 3	Multimode fiber 105/125 µm NA=0.22
Port 2	8/125 µm DCF NA=0.14/0.46
Port 4	8/125 µm DCF NA=0.14/0.46
Fiber pigtail length	> 750 mm

➢ Specifications subject to change without notice.

Optical Performance Specifications

PARAMETERS[1]		MIN	MAX		NOTES	PDR
Operating Wavelength – Signal	1530-1560	-	-	nm		
Operating Wavelength – Pumps	900-1000	-	-	nm		
Maximum Insertion Loss – Signal		-	0.35	dB	P2-4	*
Maximum Insertion Loss[2] – Pumps		-	0.5	dB	P1-4 and P3-4	*
Optical Return Loss[2] - Pump		35	-	dB	P1-1 and P3-3	*

[1] Parameters are specified at room temperature
[2] Fully filled conditions